CAPACITY FADE ESTIMATION FOR LI-ION BATTERY PACKS

by

Suvrat Ramasubramanian

APPROVED BY SUPERVISORY COMMITTEE:

Stephen Yurkovich, Chair

Nicholas Gans

Justin Ruths

Babak Fahimi

Copyright © 2017

Suvrat Ramasubramanian

All rights reserved

I dedicate this work

to my family, my advisor and my friends,

who supported me through these years

CAPACITY FADE ESTIMATION FOR LI-ION BATTERY PACKS

by

SUVRAT RAMASUBRAMANIAN, BS

THESIS

Presented to the Faculty of

The University of Texas at Dallas

in Partial Fulfillment

of the Requirements

for the Degree of

MASTER OF SCIENCE IN

ELECTRICAL ENGINEERING

THE UNIVERSITY OF TEXAS AT DALLAS

December 2017

ACKNOWLEDGMENTS

First and foremost, I would like to thank my advisor, Dr. Steve Yurkovich, for giving me the opportunity to work in his lab. His patience, guidance and support helped me accomplish my research and Master of Science degree during the two years at The University of Texas at Dallas. He motivated me to push my limits and achieve my goals.

Dr. Nick Gans gave me the opportunity to begin my research at The University of Texas at Dallas over the summer, for which I am grateful. He was also the first professor I got in touch with and he advised me throughout the initial phase of graduate school.

I would like to thank Dr. Nick Gans and Dr. Justin Ruths for serving on my examination committee. I would like to thank Dr. Babak Fahimi for agreeing to serve on my examination committee at such short notice. The financial support of the research by the Department of Systems Engineering, The University of Texas at Dallas is greatly appreciated.

I would like to thank my labmates Manav Jain and Manish Ramaswamy for their guidance and expertise with the research at the Energy Storage Systems Lab. This research wouldn't have been possible without the help of my labmates Sushant Chauhan and Moinak Pyne for collecting the test data every single day. A special thanks to OSU-CAR for providing the their test data for this research, I appreciate their generosity. I express my sincere gratitude to Rasika Katakkar for the discussions that helped me solve the problems I faced during the course of my research. I would also like to thank all my friends I made over the two years who made the journey as grad student all the more memorable.

Finally, I would like to thank my family for their continuous support. I dedicate my thesis to them. I would like to thank my mom, Rajalaskhmi, for her constant words of encouragement and support that helped during my academics and research. It would not have been possible to make it this far without their sacrifices.

November 2017

CAPACITY FADE ESTIMATION FOR LI-ION BATTERY PACKS

Suvrat Ramasubramanian, MSEE
The University of Texas at Dallas, 2017

Supervising Professor: Stephen Yurkovich, Chair

As the electric vehicle market is growing at a rapid pace, the need for accurate state of charge (SOC), state of health (SOH) estimation of the battery pack is required. Moreover, the battery management system should be able to estimate the capacity precisely with limited data from the vehicle. Currently, the different tests performed on the battery take from several hours to a few days to collect the data necessary for such estimation. In order to achieve precise OCV-SOC curves, characterization tests are executed at lower C rates from 100% to 0% SOC, which requires prolonged testing time. Additionally, more data takes longer time to process and train the system for estimating the battery states. This would prove inefficient for practical implementation. Therefore, carrying out tests at much higher C rates and reducing the SOC range will considerably reduce the time required for characterization. This thesis aims to model, predict the open circuit voltage (OCV) curve for incremental capacity analysis (ICA), and estimate capacity fade in Li-ion battery packs using relatively few data points. The study is carried out for battery packs at various temperatures.

TABLE OF CONTENTS

ACKNOWLEDGMENTS v
ABSTRACT vi
LIST OF FIGURES ix
LIST OF TABLES xi
CHAPTER 1 INTRODUCTION 1
1.1 Introduction 1
1.2 Battery Capacity Degradation 2
1.3 Battery Testing 4
1.3.1 Battery Type 4
1.3.2 Testing Equipment 5
1.4 Testing Profiles 9
1.4.1 Characterization Test 10
1.4.2 mini Reference Performance Test (mRPT) 11
1.4.3 Drive Cycle test 13
1.5 Objective 16
CHAPTER 2 INCREMENTAL CAPACITY ANALYSIS 17
2.1 Introduction 17
2.2 Incremental Capacity Analysis 17
2.3 OCV-SOC Model 22
2.4 Summary 26
CHAPTER 3 CAPACITY FADE ESTIMATION FOR TURNIGY BATTERY PACKS 27
3.1 Implementation of ICA on OCV model 27
3.2 Capacity estimation for $Q_i$test data 28
3.2.1 Temperature of 0°C 30
3.2.2 Temperature at 10°C 35
3.2.3 Temperature at 25°C 39
3.2.4 Temperature at 50°C 43
3.3 ICA Calculations 47

3.4 Implementation of ICA on mRPT test data 48
3.5 Capacity Estimation for mRPT data 50
3.6 Summary 52
CHAPTER 4 LG CHEM BATTERY 53
4.1 Introduction 53
4.2 Testing Profiles 53
4.2.1 Aging Cycle 54
4.2.2 Capacity test 55
4.2.3 HPPC Test 55
4.3 Implementation of ICA on Capacity Test 56
4.4 Capacity Estimation Using Full Data Sets 56
4.5 Reduced Data: Implementation of ICA 61
4.6 Capacity estimation for rHPPC test 62
4.7 Summary 64
CHAPTER 5 CONCLUSION AND FUTURE WORK 65
5.1 Conclusion 65
5.2 Contributions 67
5.3 Future Work 67
REFERENCES 69
BIOGRAPHICAL SKETCH 71
CURRICULUM VITAE

LIST OF FIGURES

1.1 Loss of lithium ion in the battery during charge cycles. Figure from (Vetter et al., 2005) . . . 3
1.2 Turnigy battery pack . . . 5
1.3 Cycling Station . . . 6
1.4 Thermocouple T-Type . . . 7
1.5 CSZ Temperature Chamber . . . 8
1.6 Turnigy battery pack inside temperature chamber . . . 9
1.7 Current plot at different temperatures . . . 11
1.8 OCV-SOC curve at different temperatures . . . 12
1.9 Current plot for mRPT . . . 13
1.10 Voltage plot for mRPT . . . 14
1.11 Voltage curve for Drive Cycle . . . 15
1.12 Current plot for Drive Cycle . . . 15
2.1 Different stages in LiC_6. Figure from (Groot, 2012) . . . 17
2.2 Various stages corresponding to the SOC range for LiC_6. Figure from (Groot, 2012) . . . 18
2.3 Capacity vs Voltage and ICA vs Voltage plot . . . 19
2.4 Comparison of OCV-SOC and ICA curves of different Li-ion battery. Figure from (Zhang et al., 2016) . . . 21
2.5 OCV-SOC curve . . . 23
2.6 Comparison of the OCV curve using the model equations . . . 25
3.1 V-Q curve for Model 1 at 0°C . . . 31
3.2 ICA curve for Model 1 at 0°C . . . 31
3.3 V-Q curve for Model 2 at 0°C . . . 32
3.4 ICA curve for Model 2 at 0°C . . . 32
3.5 V-Q curve for Model 3 at 0°C . . . 33
3.6 ICA curve for Model 3 at 0°C . . . 33
3.7 V-Q curve for Model 1 at 10°C . . . 35
3.8 ICA curve for Model 1 at 10°C . . . 35

3.9 V-Q curve for Model 2 at 10°C . . . 36
3.10 ICA curve for Model 2 at 10°C . . . 36
3.11 V-Q curve for Model 3 at 10°C . . . 37
3.12 ICA curve for Model 3 at 10°C . . . 37
3.13 V-Q curve for Model 1 at 25°C . . . 39
3.14 ICA curve for Model 1 at 25°C . . . 39
3.15 V-Q curve for Model 2 at 25°C . . . 40
3.16 ICA curve for Model 2 at 25°C . . . 40
3.17 V-Q curve for Model 3 at 25°C . . . 41
3.18 ICA curve for Model 3 at 25°C . . . 41
3.19 V-Q curve for Model 1 at 50°C . . . 43
3.20 ICA curve for Model 1 at 50°C . . . 43
3.21 V-Q curve for Model 2 at 50°C . . . 44
3.22 ICA curve for Model 2 at 50°C . . . 44
3.23 V-Q curve for Model 3 at 50°C . . . 45
3.24 ICA curve for Model 3 at 50°C . . . 45
3.25 Voltage range for area integration . . . 47
3.26 Voltage Points from mRPT test . . . 49
3.27 OCV curve for nonlinear polynomial model . . . 51
3.28 ICA curve for nonlinear polynomial model . . . 51
4.1 CD-CS curve for LG Chem cell. Figure from (Cordoba-Arenas et al., 2015) . . . 54
4.2 OCV curve for Model 1 . . . 57
4.3 ICA curve for Model 1 . . . 57
4.4 OCV curve for Model 2 . . . 58
4.5 ICA curve for Model 2 . . . 58
4.6 OCV curve for Model 3 . . . 59
4.7 ICA curve for Model 3 . . . 59
4.8 OCV data points from rHPPC test . . . 61
4.9 OCV curve from rHPPC test . . . 63
4.10 ICA curve from rHPPC test . . . 63

LIST OF TABLES

2.1 OCV model equations 24
3.1 Capacity estimation calculation for 0°C 34
3.2 Capacity estimation calculation for 10°C 38
3.3 Capacity estimation calculation for 25°C 42
3.4 Capacity estimation calculation for 50°C 46
4.1 Calculation for capacity test data 60
4.2 ICA calculation for rHPPC test data 64

CHAPTER 1

INTRODUCTION

1.1 Introduction

State of health (SOH) estimation for Lithium-ion (Li-ion) batteries has become an important topic of research in the recent past. Electric vehicles (EVs) like Tesla's Model S and Model X, Toyota's Prius HEV, and Nissan's Leaf have revolutionized the automotive industry by providing an alternative drive-train that performs well compared to fuel based drive-trains. Considering the rapid depletion of oil wells and the rise in oil prices in the world, along with the growing concern regarding the environmental problems due to the increase in global warming attribued to pollution, using a battery for power generation in vehicles with or instead of internal combustion engines has given the automotive industry alternatives.

There are different categories of EVs such as Tesla which runs fully on battery power while Hybrid Electric Vehicles (HEVs) and Plug-in Hybrids (PHEVs) use a combination of internal combustion engines and electric motors for power generation. The electric motors in the EVs provides extra driving mileage and improved performance, making them a desirable choice for the automotive consumers. However, challenges such as reliability, cost of operation, maintenance and performance have made it necessary to investigate and accurately predict the life and performance of the battery power sources (Scrosati and Garche, 2010). To understand the characteristics of the battery it is important to achieve the relation between its open circuit voltage (OCV) and its state of charge (SOC). This relation holds important information regarding the non-linear characteristics of the battery. Over the years, extensive research has been done on the estimation of SOC of the battery (Dubarry et al., 2007), and the OCV-SOC curve modeling to predict the available charge in the battery (Dubarry and Liaw, 2009). This has given good insight on the effect of rate of charge and discharge on the battery. However, there is a further need to understand the limitation of the battery pack

and its aging characteristics in order to make the most of the available capacity in these batteries.

1.2 Battery Capacity Degradation

A key drawback of using Li-ion based battery packs is safety and hence it is imperative to keep the battery SOC within a pre-specified range. If the battery is overcharged it can lead to fire hazard due to thermal runaway (Carnovale, 2017), (Wang et al., 2012). In this thesis, SOC and SOH estimation constitute the two most important functions of the battery management system (BMS), (Lu et al., 2013), where SOC is defined as the percentage of maximum charge present inside a battery at a particular time, and SOH is defined as amount of power delivered by the battery in its current state compared to that of a fresh battery (Weng et al., 2013). SOH corresponds to the degradation of battery which is indicated by the loss of capacity. SOH monitoring consists of capacity fade and internal resistance of the battery (Ramadass et al., 2003). To ensure longer duration of the battery's life it is important to be able to measure or estimate the capacity fade accurately.
Various factors affecting the loss of capacity can be listed as:

- Charge rate (C rate)
- Temperature
- Depth of discharge (DoD) and charge/discharge cycles

Although there are several factors that affect capacity loss, these are most important to this research. Constant charging and discharging of the battery at high C rates can cause the battery to lose its capacity much faster (Groot, 2014). Temperature plays a crucial role in capacity fade when the battery is exposed to extreme temperature ranges. A Li-ion battery is known to give an optimal performance at around 20°C (BatteryUniveristy, 2017). The

capacity fade is observed to be faster at extreme low temperatures due to loss of lithium ions. That is, as the temperature lowers the process of lithium ion diffusion slows down, thereby adversely affecting the lithium ion deposit. Hence, after each run the deposits reduce further leading to loss in capacity. However, at extremely high temperatures capacity fade is faster due to formation of solid electrolyte interface (SEI) layer and rise in impedance. Other factors that affect the battery capacity requires description of the cell chemistry, which is beyond the scope of this thesis. Several published papers on capacity fade estimation have shown that the nonlinear characteristic of the battery can be observed in the OCV-SOC curve. The capacity loss mechanism in a battery can be attributed to different stages of operation. Lithium ion batteries are usually operated in the SOC range of 90% to 50%. Capacity fade is observed to be higher in the lower SOC ranges.

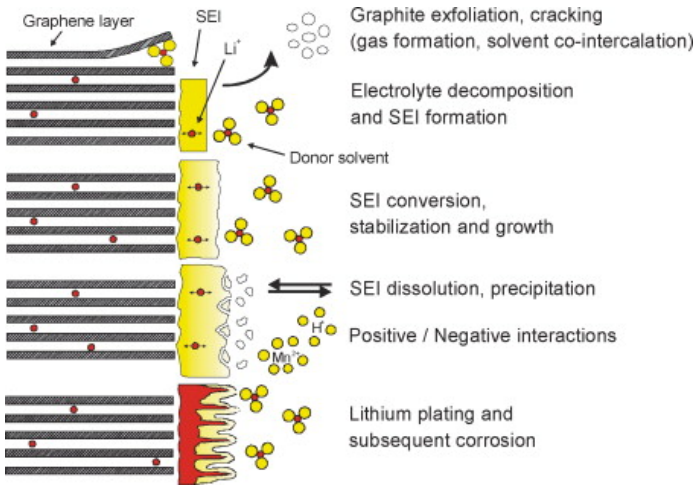

Figure 1.1: Loss of lithium ion in the battery during charge cycles. Figure from (Vetter et al., 2005)

Typically, the loss in capacity is due to a loss of active material or a loss of lithium ions during the charge/discharge cycles (Groot, 2012). The loss of lithium ions can be seen as a result of the formation of SEI layer or Li-ion plating formation at the anode electrode. (Vetter et al., 2005) shows that while aging due to the loss of the active electrode material can vary

with the choice of electrode, most of electrodes have similarities wherein the electrochemical properties of the electrode undergo a significant change (see Figure 1.1).

1.3 Battery Testing

1.3.1 Battery Type

Capacity fade estimation requires sufficient data to understand the characteristics of the battery and factors affecting its capacity. This requires that the battery be cycled continuously through various tests from the Beginning of Life (BOL) to its End of Life (EOL). The lithium polymer (Li-Po) batteries are the most commonly used battery in the industry due to their comparatively slower charge loss, and high energy density. This enables them to be lighter and compact as compared to a lead acid battery.

A battery pack manufactured by Turnigy has been used to generate testing data for much of this thesis. This Li-Po battery is usually used for lower energy and power density applications such as for RC toy cars. The idea behind using this battery was to cycle the battery continuously for a relatively short period of time and reduce the capacity to a significant level in order to understand the characteristics of the capacity fade in the battery. Generally, an automotive grade Li-Po battery lives for several years and cycling them to their EOL would take years of testing. For instance, a Tesla car battery pack may take several years to drop 20% of its capacity from BOL. Thus testing data from the Turnigy battery cycled from its BOL to EOL is processed and analyzed to understand its characteristics and factors effecting the capacity fade. These results are then extended to estimating the capacity fade in higher quality test data from automotive grade cells using the same processing and analysis methods. This will be discussed further in the remainder of the thesis.

The battery shown in Figure 1.2 used for the experiment has a nominal capacity of 2.2Ah. The pack has three cells in 3S1P configuration, that is three cells in series connection. Each

cell in the battery pack has an operating voltage between 2.75V and 4.2V and nominal voltage of 3.7V. The battery pack has an operating voltage between 8.25V and 12.5V and nominal voltage 11.1V.

Figure 1.2: Turnigy battery pack

1.3.2 Testing Equipment

For this thesis, the setup used consists of a cycling station, a temperature chamber and the associated software tools. The cycling station was assembled by Car Technologies, LLC. The company is known for its testing, research and development of automotive grade batteries technologies and it works in collaboration with Center for Automotive Research at Ohio State University (OSU-CAR).

Cycling Station

The cycling station as shown in Figure 1.3 is designed to run previously designed current profiles for charging and discharging the cells and the battery pack. In discharge mode it is capable of producing currents as large as 100A which could generate large amount of heat (Guo, 2015). Therefore, in the absence of the BMS operating in the cycling station, certain precautions and safety measures are needed to prevent fire hazards or damage to the battery in case of over-charging and over-discharging. For this reason, the cycling station is equipped with specific control software to keep the battery within its safe operating range.

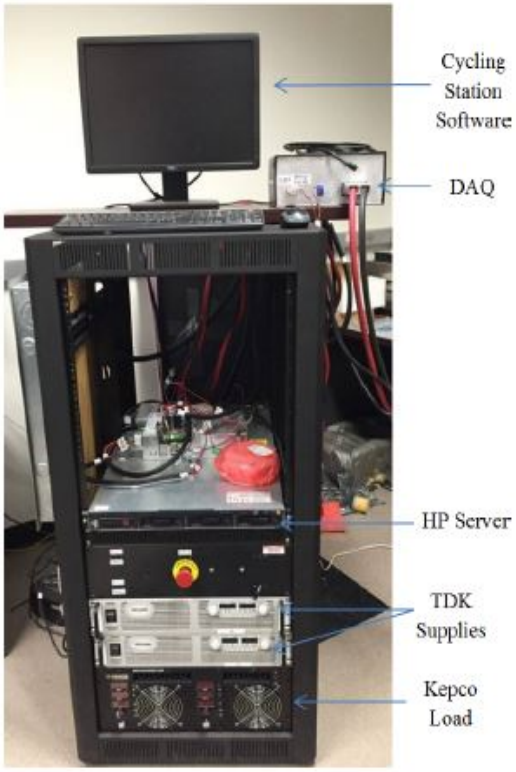

Figure 1.3: Cycling Station

In case of unpredictable situations where the battery is likely to hit over-voltage, under-voltage, over-current, under-current, temperature outside its operating range conditions, the software triggers the emergency stop (E-STOP) which shuts down the test. In addition, the station is also equipped with a smoke detector which will enable the emergency stop when required.

Cycling Station Hardware

Following are the hardware equipment in the cycling station:

1. ***Data Acquisition Device (DAQ)*** is a National Instruments *NI USB-6008*, USB powered device. The DAQ shown in the Figure 1.3 is placed in a shielded metal box to minimize the magnetic interference from other devices. The voltage, current and temperature data from the battery is sampled by the DAQ and fed back to the server

where the software evaluates the data and plots the real time results. The feedback from the DAQ is also used to operate E-STOP.

2. ***HP server*** is used to govern the customized software for controlling the power supply, load and data acquisition devices. It runs on Red Hat Linux operating system.

3. ***TDK Lambda GEN8-400*** is a high current power supply that is used for charging the cells or battery pack depending on the configuration and the test profiles run. In the cycling station, two of these power supplies are connected in series to provide max voltage of 16V and current of about 400A.

4. ***Kepco Load EL 3k-25-400DG*** is a programmable load through which the cell or battery pack is discharged. The load is rated at 3000W power, 25V voltage and 400A max current.

5. ***Thermocouple T Type*** shown in Figure 1.4, is a temperature sensor used on the cycling station for real time temperature sensing of the battery in the temperature chamber. The thermocouple helps in recording the thermal behavior of the battery during the charge and discharge phase. Most importantly the temperature measurement is used for determining conditions for E-STOP.

Figure 1.4: Thermocouple T-Type

Temperature Chamber

The temperature chamber used for battery testing is a Cincinnati Sub-Zero (CSZ), MicroClimate®

Benchtop Test Chamber shown in Figure 1.5. The chamber is capable of handling single stage temperature ranging from -30°C to +190°C (-22°F to +375°F). With a *CSZ EZT-430i Touch Screen Controller*, the chamber offers numerous ways for the user to control the temperature manually or with external devices such as a smart phone or using a windows-based navigation.

Figure 1.5: CSZ Temperature Chamber

The Turnigy battery is connected to the power cables for the current to flow as shown in Figure 1.6. The voltage sensing cable and thermocouple wire are also connected to the battery inside the temperature chamber. The cables and the wire are inserted into the chamber from the left side through a hole. A soft sponge is placed at the hole for isolation in order to eliminate thermal leakage from the chamber.

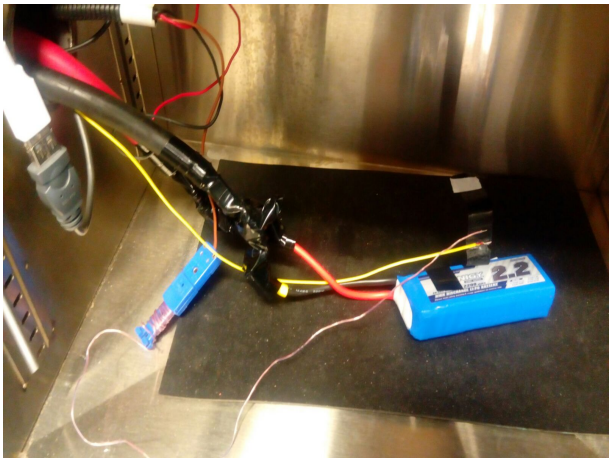

Figure 1.6: Turnigy battery pack inside temperature chamber

Cycling Station Software

The software used for running the test is a LABVIEW-based GUI developed by CarTech for managing the operations of the cycling station.

The user interface of the software is where all the operation for the testing is performed. All the necessary files for the test, based on the test profile being run, are loaded into the software. Once a test profile is created and saved using SAVE SETUP, the software lets the user reload the file using the LOAD SETUP button from the folder where all the preprogrammed files are saved. The test is started or stopped using the START or STOP buttons, respectively. The voltage, current and temperature data is stored in real time and saved in a binary file. This binary file is down sampled using DATA VIEWER program and saved as a .csv file. The .csv file is then loaded in MATLAB for data analysis and further processing.

1.4 Testing Profiles

The testing profiles are designed for the purpose of cycling the battery from its BOL to EOL. However each testing profile is designed for a specific reason. The tests executed during each cycle are characterization test or Q_i test, mini reference performance test (mRPT) test and

a drive cycle. The characterization tests are run at the beginning of each test cycle from SOC 100% to 0%. Since the testing is done at low C rate and at constant current, the characteristic voltage curve resembles an OCV curve. The mRPT test profile is a pulse test similar to a hybrid pulse power characterization (HPPC) but run at higher C rates. The test is named mini RPT because the SOC ranges from 100% to 50%. The mRPT is performed for two main reasons: the SOC range is half of that of an HPPC or a characterization test, and the time to execute the test reduces significantly which is crucial for capacity estimation method. The drive cycle plays an important role in the cycling of the battery since the test profile is designed to replicate the discharging and charging of the battery when the EV is under normal use. Current pulses at varying C rates and varying levels have a large impact on the capacity loss. Each test profile will be discussed further in detail.

1.4.1 Characterization Test

OCV is the steady state voltage measured during the rest phase after charge or discharge, when there is no current flowing through the battery. The OCV curve is represented with respect to SOC, where the SOC ranges from 0% to 100%. Characterization test is performed on the battery at low C rates and at continuous charging current to get the OCV-SOC curve.

The characterization test when performed at lower C rates produces an accurate OCV-SOC curve. For the Turnigy battery with a nominal capacity of 2.2Ah, the C rate of 1C corresponds to 2.2A charging current. A characterization test consists of a continuous discharge at 2.2A followed by an hour long rest and continuous charge at 2.2A. Since the test is run at constant 1C rate, the time taken for the battery to completely discharge from 100% to 0% SOC is about an hour. Therefore, nominally for a 2.2Ah battery discharged at 1C rate will discharge completely in one hour with current at 2.2A.

The voltage curve is represented in time. For the experiments in this thesis, the discharge curve is taken as OCV-SOC curve. To get an OCV-SOC curve the discharge curve is normalized to the SOC from 0% to 100%. The characterization test is run at different temperatures

(0, 10, 25 and 50°C). Figures 1.7 and 1.8 show the discharging current and voltage plot, respectively, for different temperatures. The voltage curve shows the effect for temperature on the battery, where we observe that the battery voltage drops faster a 0°C and the battery performs the best at temperature around 25°C. The voltage curves are relatively close to the actual OCV-SOC curve. As the C rate is reduced further, such voltage curves will closely approximate the true OCV-SOC curve.

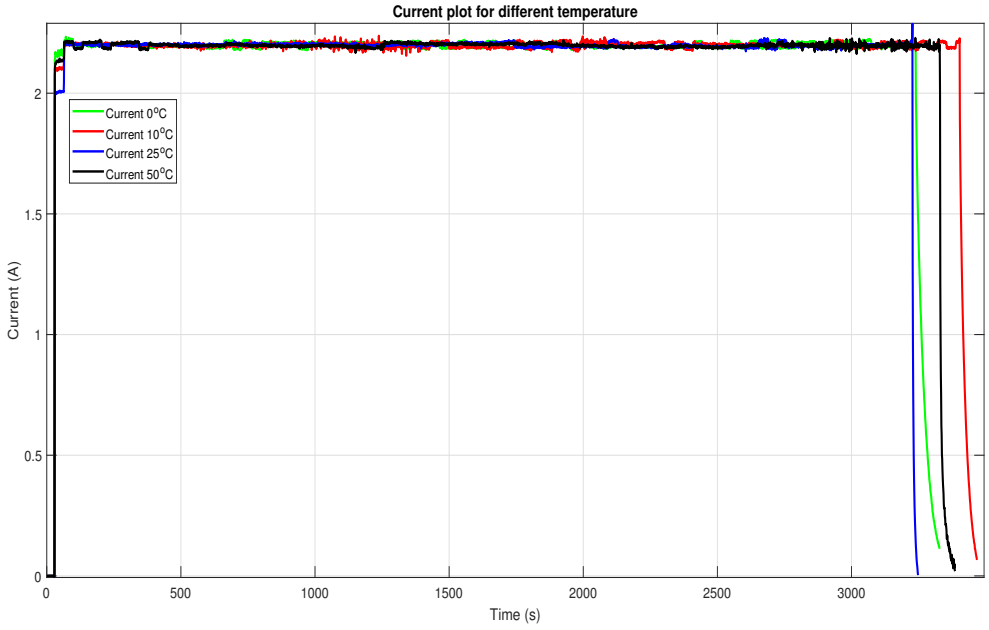

Figure 1.7: Current plot at different temperatures

1.4.2 mini Reference Performance Test (mRPT)

Reference Performance Tests (RPT) are a set of tests performed at periodic intervals during the life of the battery to measure the performance degradation of the battery under test. A typical RPT consists of a characterization test followed by a HPPC test. These tests are run at low C rates (C/1, C/3, C/5) depending on the battery capacity. The RPT data stored in the DAQ is processed and analyzed for battery degradation. First, the voltage values at the

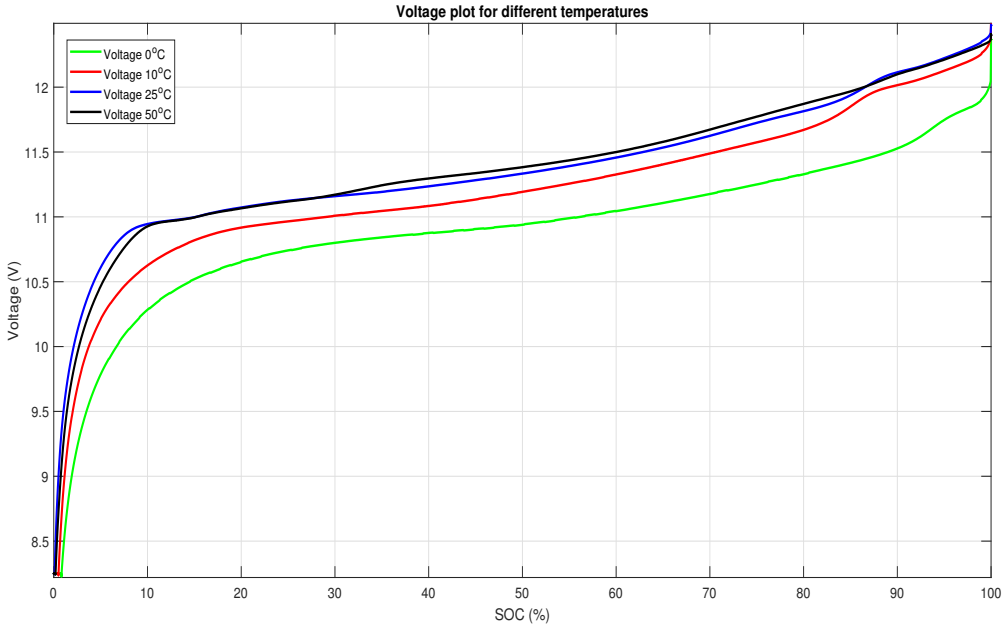

Figure 1.8: OCV-SOC curve at different temperatures

end of each rest period are isolated to get the required points at every 10% drop in SOC. Then the voltage drop across the internal resistance is summed with the voltage value to get the desired OCV points. These OCV points are then fitted to a curve to get the estimated OCV-SOC curve. The OCV-SOC curve is then used for capacity fade estimation.

The mRPT executed for the Turnigy battery is a kind of HPPC test. HPPC test is considered as alternative method of running characterization test with 10% SOC change, from 100% to 0% for each pulse at low C rates. HPPC tests have shown to give similar results as the characterization test. mRPTs are performed at higher C rates with SOC change from 100% to 50%. The battery pack is discharged to 50% SOC at a 10C pulse with each current pulse having a duration of 36 secs. The discharging is followed by 1800 secs of rest where the voltage rises to the actual OCV value. A 5C constant current charges the battery to 100% SOC. Since the mRPTs discharge the battery to 50% SOC as compared to the $Q_i$test of full discharge, the execution time of mRPT is less.

Figures 1.9 and 1.10 show the current and voltage plot, respectively, for a single mRPT discharge/charge cycle. The voltage curve shows the drop in the voltage as the pulse is applied. During the rest phase, the current is zero and the voltage can be seen rising to the OCV value. As it approaches the OCV value, the voltage curve settles and becomes constant. Each OCV value at the end of the rest phase is taken as the voltage value corresponding to the SOC point.

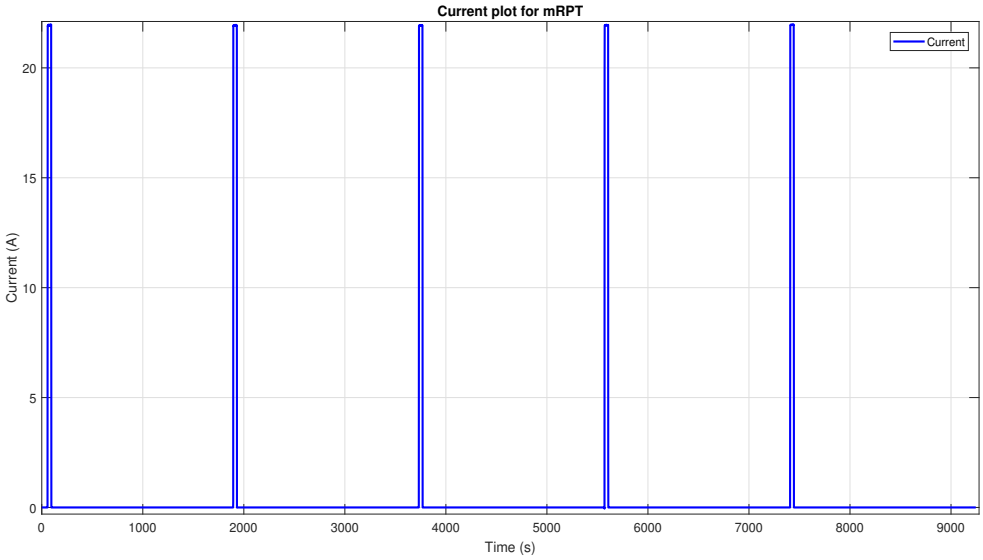

Figure 1.9: Current plot for mRPT

1.4.3 Drive Cycle test

Capacity fade of a battery pack in an electric vehicle varies based on the usage. The battery undergoes a number of charge and discharge cycles at different rates depending on the driving pattern and charging rates. During this the battery could be operated at extreme rates which significantly affect the capacity. In order to replicate such conditions, the battery under test is made to go through a similar profile, where the battery is discharged and charged at higher C rates thus hitting it really hard. This is achieved by the drive cycle profile. The Turnigy

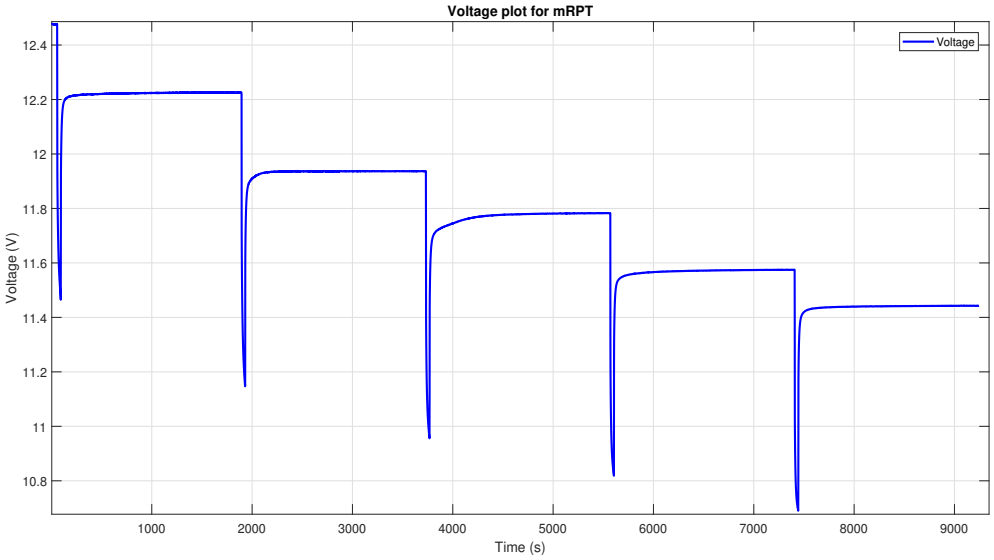

Figure 1.10: Voltage plot for mRPT

battery pack has a maximum discharge rate of 20C with a 10 min peak pulse discharge at 30C. The peak charge rate is limited to 10C for safety.

The drive cycle profile consists of 8 discharge pulses for a specific duration. The pulse duration is calculated based on the battery capacity and the C rate. As mentioned earlier the battery discharges from 100% to 0% SOC in 1 hour or 3600 sec. Therefore,

$$1\text{C} \rightarrow 3600 \text{ secs} \Rightarrow 10\text{C} \rightarrow 360\text{secs}$$

$$10\text{C for } 10\% \text{ SOC drop} \rightarrow 36\text{secs}.$$

Therefore, each pulse is applied for a period of 36 secs at 10C and 18 secs for 20C. This profile is run on constant current mode where the current supply switches immediately after the specified pulse duration is reached.

Figures 1.11 and 1.12 show the current and voltage plot, respectively, for a single drive cycle. Each of the 8 pulse sets are shown to consist of 3 discharge pulses at varying C rates, a rest phase and 3 charge pulses at different C rates. The effect of each pulse set can be observed from the voltage curve. The impact of the drive cycle is such that the voltage

gradually varies from maximum to minimum for each pulse set. This factors a lot in the degradation of battery capacity.

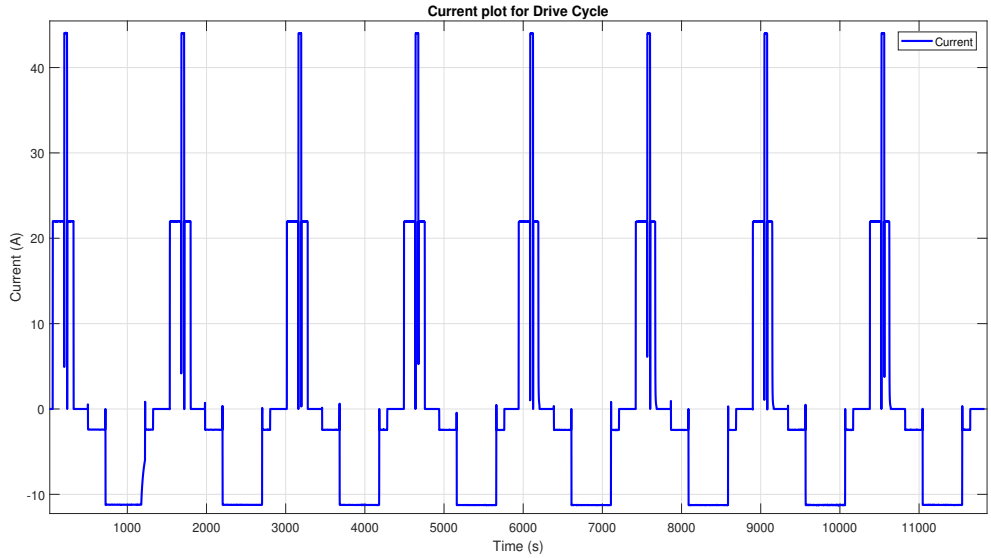

Figure 1.11: Voltage curve for Drive Cycle

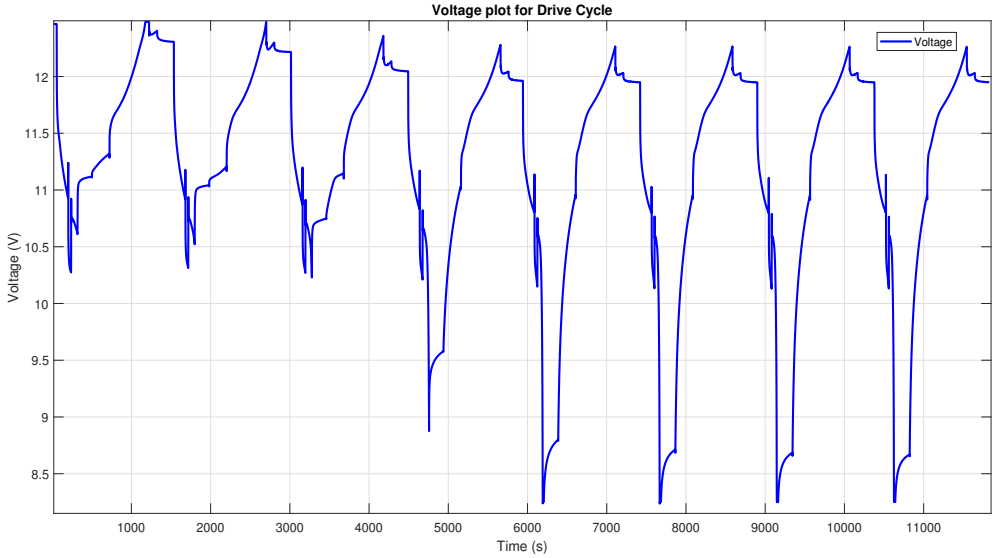

Figure 1.12: Current plot for Drive Cycle

1.5 Objective

SOH estimation is an integral part of the BMS and accurate estimation of the battery's SOH is important to ensure safe and efficient utilization of the battery for driving an EV. A good estimation technique to predict the loss in battery capacity is desired, doing so with fewer test data. In this thesis, we identify an OCV model to obtain a good estimate of the OCV-SOC curve that captures the characteristics of the curve using fewer data points. A technique using incremental capacity is applied to the estimated OCV curve to accurately predict the capacity fade in the battery.

A strong motivation for using less amount of data from mRPT test comes from accurate estimation of capacity using supervised learning shown in (Pyne et al., 2017). In this paper, the author uses data points from mRPT test and predicts the capacity fade observed in a battery at different temperatures. The objective of this thesis is to use the technique of incremental capacity on mRPT test data for accurate estimation of capacity fade in a battery.

The remaining chapters in this thesis are set as follows. Chapter 2 describes the estimation technique used for this thesis and the OCV models for the OCV-SOC curve. In Chapter 3 we discuss capacity estimation for the Turnigy battery pack using two different testing profiles. Chapter 4 discusses similar results for the LGChem cell, which is of higher quality. The last chapter compares the two types of batteries and also discusses future work possible for this research.

CHAPTER 2

INCREMENTAL CAPACITY ANALYSIS

2.1 Introduction

In this chapter we will discuss the incremental capacity analysis (ICA) technique for capacity fade estimation and review the literature to summarize the effectiveness of the estimation technique. Additionally, we will discuss several OCV model equations that will be used for the analysis. The technique is implemented on the Turnigy battery pack and LG Chem cell test data in subsequent chapters, where results are presented.

2.2 Incremental Capacity Analysis

The ICA is an analysis technique which is widely used for observing the decrease in capacity as the battery is cycled to imitate the aging process. During the intercalation/de-intercalation of lithium ion, the battery goes through different stages. Figure 2.1 shows different stages of lithium ion accumulation at the cathode in LiC_6.

The table in Figure 2.2 shows the range of SOC corresponding to the different stages in

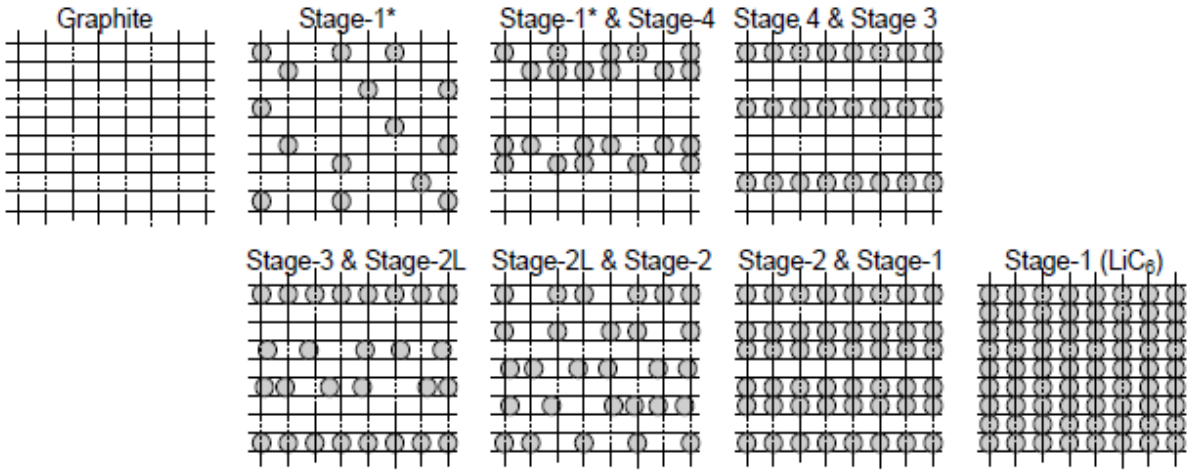

Figure 2.1: Different stages in LiC_6. Figure from (Groot, 2012)

the battery. The SOC range of 50% to 95% is the region where the lithium ion battery characteristically shows a plateau in the OCV curve. This region is typically the operating region of the li-ion battery. Similar characteristics can be observed in other chemistry of li-ion batteries. Each of these stages in the battery translates to a plateau in the OCV-SOC

SOC Range [x in Li_xC_6]	Graphite Phase
0-0.04	Stage-1(dilute)
0.04-0.12	Stage-1(dilute) & stage 4
0.12-0.20	Stage-4 & Stage-3
0.20-0.25	Stage-3 & Stage-2(liquid)
0.25-0.50	Stage-2(liquid) & Stage-2
0.50-1	Stage-2 & Stage-1

Figure 2.2: Various stages corresponding to the SOC range for LiC_6. Figure from (Groot, 2012)

curve. The ICA curve show peaks corresponding to the plateaus in the OCV curve.

Incremental capacity (IC) is a numerical derivative of the incremental change in the capacity with respect to the incremental change in voltage (Weng et al., 2016). Voltage points considered for this calculation correspond to the estimation of OCV data obtained from the OCV model. The capacity data points are generated by the summation of the current at each time period for the testing data stored after down sampling to 1 Hz. Therefore,

$$\begin{aligned} Q_{j+1} &= Q_j + i_j \Delta t \Rightarrow \delta Q = Q_{j+1} - Q_j \\ V_j &= OCV_j \Rightarrow \delta V = V_{j+1} - V_j \\ \therefore IC &= \frac{\delta Q}{\delta V} \end{aligned} \tag{2.1}$$

where Q_j, V_j *and* i_j are accumulated charge capacity, voltage and current at time step j, respectively, and Δt is the sample time. δQ *and* δV correspond to the increments of accumulated charge capacity and increments of voltage, respectively, and their ratio gives the ICA points. The change in the voltage in the plateau region of the OCV curve is small

corresponding to the change in the capacity value in the same region, producing a large value for the derivative. This creates the peaks that we see in the ICA curve as shown in Figure 2.3 for a small region of the OCV curve. The peak is formed in the voltage region where the OCV curve forms a plateau.

The ICA curve allows us to investigate the changes in the battery cell chemistry occurring over various test cycles and record them with greater sensitivity. The ICA peaks are sensitive to the smallest changes in the capacity and voltage of the battery. The variations in peak

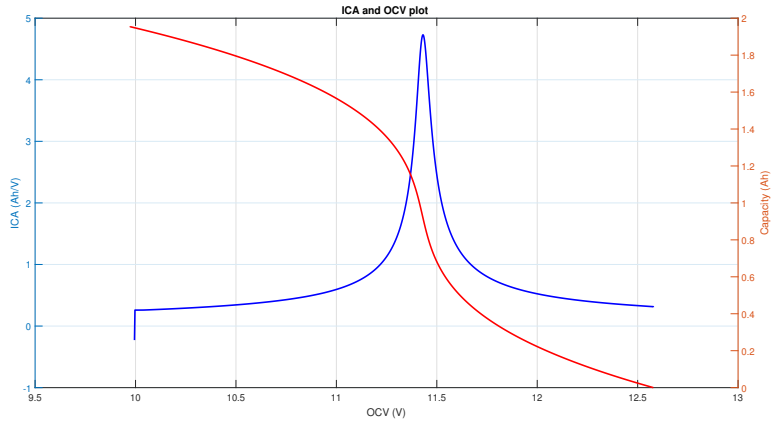

(a) OCV and ICA relation

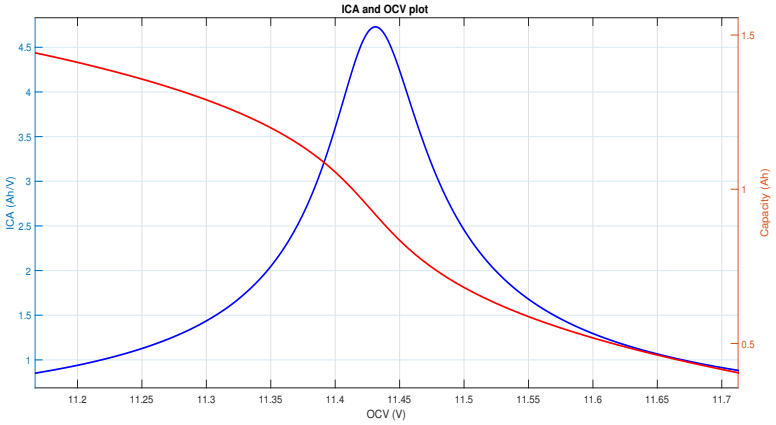

(b) OCV and ICA relation (zoomed)

Figure 2.3: Capacity vs Voltage and ICA vs Voltage plot

reveal the important information regarding the cell chemistry, over the numerous tests that

are conducted. Furthermore, the pattern of the peak evolution can be affected by several events occurring in the battery. As the battery ages, the peaks of the ICA vary in accordance with the decrease in the capacity of the battery. (Dubarry et al., 2006) shows that the variation in the peak is observed to be a decrease in the peak height and a shift of the peak after each test. The decrease in the peak height is due to loss of lithium ions and the shift in the peak is due to the loss of active material. While the loss of lithium ions could be attributed to the accumulation of Li^+ ions at the cathode and formation of SEI layer, the shift in the ICA peaks can be attributed to undercharge and under-discharge.

Because of the fact that ICA peaks depend on the nonlinear characteristics observed in the OCV curve, it can be inferred that the ICA curves vary with the OCV-SOC curve characteristics. (Zhang et al., 2016) discusses the OCV-SOC curves for different lithium ion batteries displaying their respective staging processes, shown in Figure 2.4. Furthermore, the paper discusses the ICA peaks that correspond to each staging process, thereby providing analysis for the distinct nature of different batteries. The paper compares the Li-ion batteries having different cathode material. As shown in Figure 2.4, the electrode material in each battery is composed of LNMCO-lithium nickel manganese cobalt oxide, $LiMn_2O_4$ - lithium manganese oxide, $LiFePO_4$ - lithium iron phosphate and LTO - lithium titanate. The OCV -SOC characteristics can be seen to vary a lot based on the electrode material. Figure 2.4a shows that the battery discharges/charges gradually during stage I due to the electrochemical reaction in the battery electrodes. The plateau region in the OCV-SOC curve indicates very few reactions taking place and the voltage change is negligible over a period of time. These plateaus can be seen translating to a distinct peak in the ICA curve. Each battery has different stages of lithium ion intercalation/deintercalation which results in distinct characteristics. The OCV-SOC curve captures these characteristics that display the nonlinear behavior. It is evident from Figures 2.4a, 2.4b, 2.4c and 2.4d that different OCV-SOC characteristic curves give distinct ICA curves which uniquely define the capacity

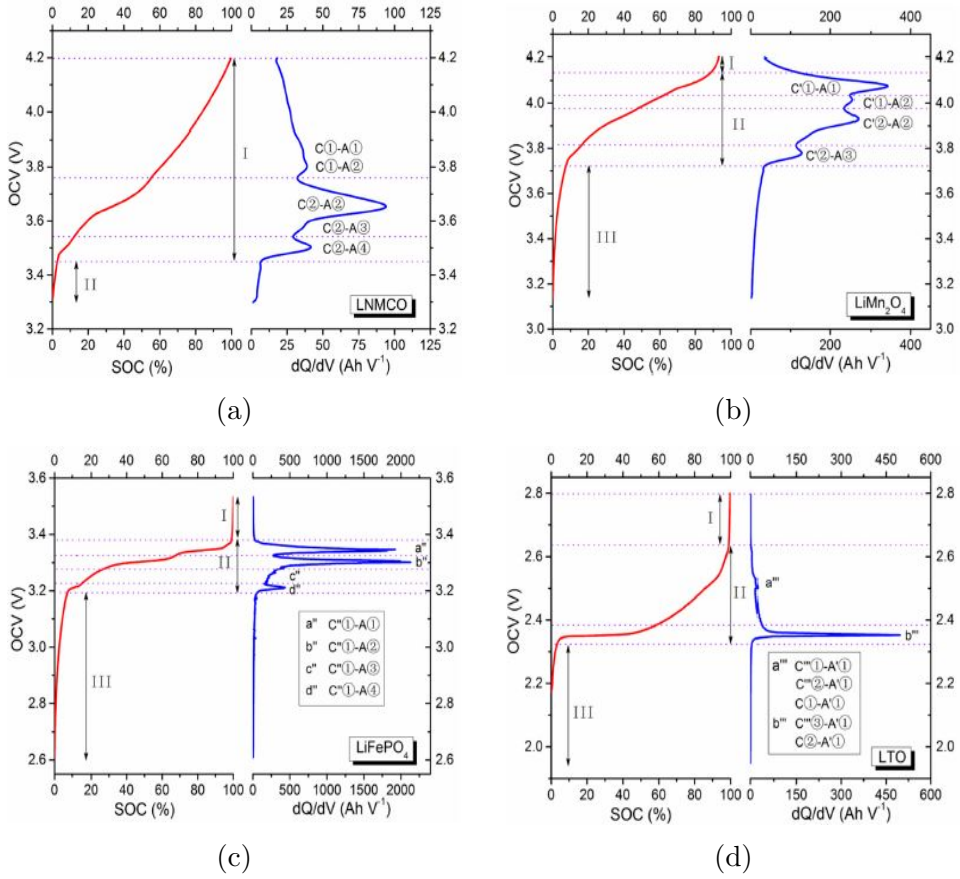

Figure 2.4: Comparison of OCV-SOC and ICA curves of different Li-ion battery. Figure from (Zhang et al., 2016)

loss in a battery, as the battery is cycled over the period of its life. Another significant detail to note here is that the cell chemistry for Figure 2.4d has a lithium titanate anode while the other batteries have a graphite anode. The electrochemical reactions in the battery are such that the OCV-SOC curve has distinct characteristics. Nonetheless, each battery has a set of three stages in the discharging/charging process.

The analysis of ICA through the ICA curve gives an illustrative idea of capacity fade and the various factors affecting it. However, a computational analysis of the ICA is desirable. The estimated area of the peak is evaluated through basic integration to calculate the accumulated capacity that leads to estimation of capacity fade.

2.3 OCV-SOC Model

Numerous research studies have shown the importance of OCV for the SOC estimation. The OCV curve plays a crucial role in the estimation of the SOC as it expresses the characteristics of the battery (Weng et al., 2014). Hence, it is important to accurately estimate the OCV-SOC curve. A small error in the OCV curve may miss some of the nonlinear characteristics of the battery thereby causing a large error in the SOC estimation. Since the OCV curve also represents the capacity fade and degradation in battery performance, it has a significant impact on the SOH estimation. Moreover, because of the inherent sensitivity in the calculation of the incremental capacity, it is critical to have a smooth and accurate representation of the OCV.

In order to predict the OCV curve accurately, it is necessary to model an equation that captures the complex behavior of the battery during the intercalation/deintercalation process and the voltage plateaus corresponding to the staging events at the anode. Over the years of research on SOC estimation, several OCV models have been developed to estimate the OCV-SOC curve (Roscher et al., 2011). Figure 2.5 shows OCV-SOC curve for the Turnigy battery at 25°C. We can observe distinct transition stages during the cell charge/discharge at around SOC 100%, 85% and 15%.

In the previous chapter, we discussed the characterization test run continuously at low C rates and at constant current. The discharge curve obtained from the test data is very close to equilibrium OCV curve (Dubarry et al., 2006), and hence is considered to be the true OCV curve. The discharge voltage data may be affected by voltage due to the internal resistance and polarization resistance. However, the curve obtained from the tests that is close to the equilibrium OCV curve can, nevertheless, be used for the parameter estimation of the OCV model. Although the OCV curve from a Q_i test is sufficient for the estimation, there is a need for an OCV model for capacity fade estimation since the test data from the Q_i test is noisy. The data for voltage and current obtained from the test is raw and unprocessed, that

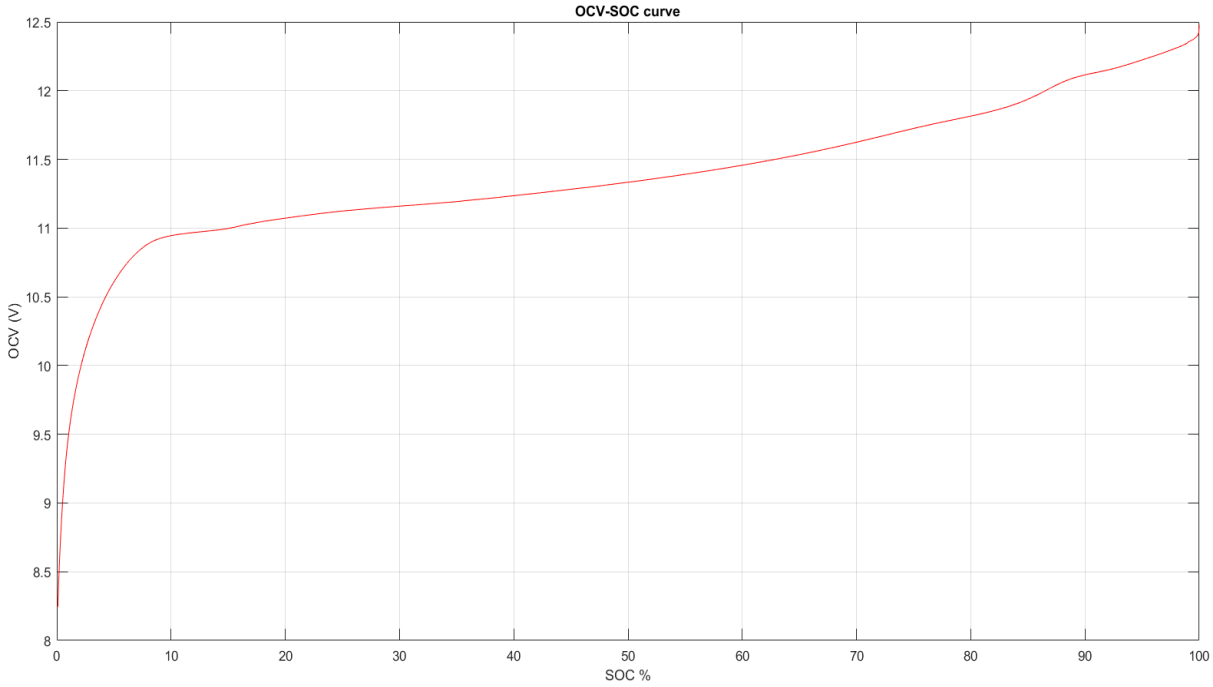

Figure 2.5: OCV-SOC curve

is, the data is not smooth for direct usage which in turn leads to erroneous calculations. In addition to this, ICA is sensitive to noise since the calculation of ICA is essentially a ratio of increments of the capacity and voltage. Any variation in the data will be translated into a stray peak in the ICA curve, due to which the precise estimation of capacity fade estimation will be futile. Therefore it is crucial to use a smooth OCV curve for the capacity estimation using IC analysis method. As a consequence, we consider ways to estimate the OCV-SOC curve. The OCV models we employ are designed to estimate the OCV curve by capturing the nonlinearities through the model parameters and at the same time provide smooth data points that can be used to calculate ICA value to achieve smooth peaks that are essential for accurate estimation of capacity fade. The OCV models used and compared in this thesis are shown in Table 2.1.

(Weng et al., 2014) was our primary source for the OCV model equations and for understanding the implementation of ICA on these equations for capacity fade estimation.

Table 2.1: OCV model equations

Model	Equation
MODEL 1: Combined	$OCV(z) = K_0 - \frac{K_1}{z} - K_2 z + K_3 ln(z) + K_4 ln(1-z)$
MODEL 2: 3rd Order	$OCV(z) = K_0 + K_1 z + K_2 z^2 + K_3 z^3$
MODEL 3: 6th Order	$OCV(z) = K_0 + K_1 z + K_2 z^2 + K_3 z^3 + K_4 z^4 + K_5 z^5 + K_6 z^6$

The OCV models discussed in the paper and used in this thesis are designed in accordance with the characteristics of the OCV curve stages discussed in the previous chapter.

The OCV-SOC model is formed using least squares estimation, since the equation is linear in the parameters, and the OCV data from the Q_0 test is used for parameter identification. The estimation problem is formulated as follows:

$$\begin{aligned} Y &= \theta^T \phi \\ \theta &= [K_1, K_2, ...K_n]^T \\ \phi &= [\phi_1, \phi_2, ...\phi_n]^T \\ \theta &= (\phi^T \phi)^{-1} \phi^T Y \end{aligned} \tag{2.2}$$

where K_i, $(i = 1, ..., n)$ are the model parameters, and Y is the test data $[y_1, y_2, ...y_n]^T$. For Model 1, $\phi = [1, \frac{-1}{z}, -z, ln(z), ln(1-z)]^T$, where z is the normalized SOC value. Model 1 shown in Table 2.1 is a combination of 3 equations. (Plett, 2004) shows that Model 1 is the combination of Shepherd model, Unnewehr universal model and Nernst model. This combination of the equations form a reasonable representation of the required information about the battery characteristics. Model 2 and Model 3 were chosen since the curves fitted using these models resembled the OCV curve and with estimated parameters, do a reasonable job of capturing the nonlinear characteristics of the battery. The model equations are a

function of z, where for Model 2 and 3 z is the SOC value calculated from coulomb counting and for Model 1 z is the normalized SOC value. The parameters are identified using the relationship given in 2.2.

Figure 2.6 shows the comparison of the OCV curve from the three models with the measured OCV curve from the test data. The curves Model 1, Model 2, Model 3 indicate

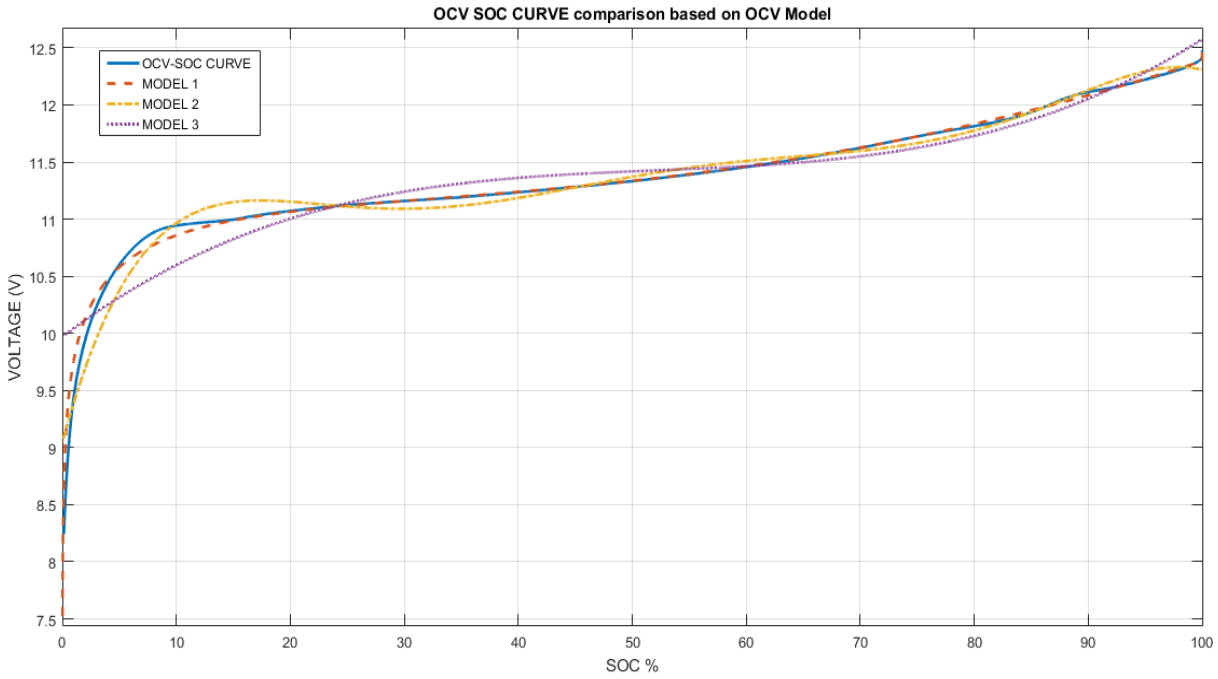

Figure 2.6: Comparison of the OCV curve using the model equations

the combined model equation, 6th order polynomial model and 3rd order polynomial model, respectively. The OCV-SOC curve estimated from the curve fit for the Model 2 seemed to give the best fit. Given the nature of the ICA calculations (explained above) and the useful range of the battery, we are most concerned about the accuracy of the curvefit in the regions where the OCV plateaus are formed, particularly in the transition regions.

2.4 Summary

In this chapter, we have introduced the ICA methodology using OCV model for the capacity fade estimation. The peak tracking technique using IC analysis is shown to be an accurate method for capacity fade estimation. The method shows the transformation of the plateaus in the OCV curve into distinct peaks which vary in height as the battery loses capacity. The OCV models used for this thesis are discussed giving an insight on the usefulness of good OCV models for estimating the OCV-SOC curves. Furthermore, the smooth data obtained from the OCV model helps in accurate analysis of the peak.

The following chapters show the implementation of the ICA curve using the OCV model for capacity fade estimation on the Turnigy battery pack and the LGChem cell.

CHAPTER 3

CAPACITY FADE ESTIMATION FOR TURNIGY BATTERY PACKS

3.1 Implementation of ICA on OCV model

In this chapter we make use of the OCV models that capture the wide flat region in the OCV curve due to the intercalation/deintercalation process and the nonlinear characteristics. In turn, information is extracted and related to the SOH of the battery using ICA. The OCV model mitigates the effect of the noise that could lead to erroneous results in addition to distorted ICA curves due to noise sensitivity.

The ICA is essentially a derivative in the form of a ratio of incremental capacity to incremental voltage. While calculating the derivative using the OCV data, it is possible for the denominator to vanish due to zero change in the voltage increments in the wide flat region of the OCV curve. This would lead to singularity in the ICA calculation. Hence, the calculation of ICA has to be done keeping the zero voltage change in mind. Generally, the voltage tolerance of the change is kept around 1mV and any change below 1mV is discarded. The ICA calculations for different models give different peaks and varying peak heights since each model captures different characteristics of the OCV curve. All the models for the ICA evaluation are tested for different temperatures.

Each battery pack underwent a series of tests during the aging process, at different temperatures. The battery testing was conducted until EOL was reached which is set at around 50% of the initial capacity. The effect of extreme temperatures is such that the battery aging increases rapidly and the battery reaches its EOL in less number of test cycles. This is attributed to the change in the chemical process at the electrodes for each temperature. Typically li-ion batteries perform best at room temperature (25°C). In order to study the effect of temperature variation on battery, aging test data from each battery is collected and IC analysis is performed. Li-ion batteries have the capability of operating in temperature range of -5°C to 50°C.

3.2 Capacity estimation for $Q_i$test data

The Q_i test data consists of a large amount of data points over the entire SOC range, i.e, 100% to 0%. For the estimation of capacity, only the discharge data is considered. The number of data points can vary depending upon the C rate at which the test is conducted. Lower C rates result in a larger number of points. For the Turnigy battery, the Q_i test is performed at 1C. Each set of tests are analyzed for capacity fade at different temperatures using the method discussed in the previous chapter.

Due to various combinations of temperatures and OCV models (Model 1, Model 2 and Model 3), we will first discuss the three OCV models and their performance and later present the results of capacity estimation for different temperatures.

Model 1: Combined Model

The combined model is the first model used in this thesis, designed as a function of battery SOC. The SOC data used for modeling is normalized. The curves shown in Figures 3.1, 3.7, 3.13 and 3.19 are voltage versus capacity curves which depict the characteristic nature of the OCV-SOC curve. These curves capture the capacity loss after each set of test cycles that the battery undergoes. However, the model is unable to reproduce the flat region of the OCV-SOC curve. Furthermore, the model curve fails to include the characteristic initial drop in the voltage.

Next, to understand the capacity fade after each test cycle set, IC analysis is performed. The OCV curve from the combined model is transformed into an ICA curve where the flat regions of the OCV curve produce peaks. For the OCV curve obtained from the combined model, we receive a single ICA peak corresponding to the operating region of 90% - 50% SOC. Since the OCV model is unable to capture the flat region of the OCV curves accurately, the ICA curves transformed, shown in Figures 3.2, 3.8, 3.14 and 3.20, from the estimated OCV curves terminate prematurely. The error in the prediction of the OCV curves are projected in the ICA curves. However, the ICA curves are observed to illustrate the capacity drop

with the decrease in the ICA peaks as the battery cycling progresses. This validates the ability of the IC analysis to track the capacity fade in the battery.

Model 2: 3rd order polynomial

The OCV model used next is a polynomial relation of the OCV with the SOC of order three. Figures 3.3, 3.9, 3.15 and 3.21 show the OCV curves obtained from the model for the different temperatures. The OCV curve from this model resembles the OCV-SOC curve for a typical li-ion battery due to the nature of the Model 2 equation, thereby making it a natural choice for OCV estimation. The OCV model captures the capacity loss in the battery and the flat region around the nominal voltage. However, the model is unable to extract all the nonlinear characteristics for different stages of operation. The OCV curves transform into a single ICA peak, illustrated in Figures 3.4, 3.10, 3.16 and 3.22.

The ICA curves for Model 2, however, show that the OCV curves perform better compared to Model 1 in estimating the OCV-SOC curve. The curve neatly depicts the fading of capacity with the reduction in ICA peaks. Formation of sharp peaks for Model 2 is due to the flatter region of the OCV curve. The change in voltage is significantly small which translates into identifiable peaks.

Model 3: 6th order polynomial

The OCV model using Model 3 is observed to fit OCV curve the best amongst the other models discussed in this thesis. The characteristic nature of the polynomial is such that it sharply captures the attributes of the OCV-SOC curve. However, this OCV curve fails to capture the initial drop in the voltage due to nonlinearity. The OCV curves obtained using Model 3 are shown in Figures 3.5, 3.11, 3.17 and 3.23.

The OCV curves from Model 3 have two prominent flat regions, as we would expect, which are the closest estimate of the actual OCV curves. The degradation in the capacity is observed in the OCV curve which is transformed into ICA peaks for IC analysis. The ICA curves have two distinct peaks as shown in Figures 3.6, 3.12, 3.18 and 3.24. The two flat

regions in the OCV curve can be interpreted as two transition stages in the li-ion intercalation and de-intercalation. Each flat region in the OCV curve is transformed into the ICA peaks around the operational voltage region. The peak formed at the higher voltage is used for the capacity calculation. The capacity value is calculated by calculating the area under the curve which is a sum of the accumulated capacity over the entire test range.

Q_0 test data from the battery is first used to estimate the parameters for an accurate BOL OCV-SOC curve using the model equations. The remaining OCV curves estimated using the parameters are then analyzed for capacity fade estimation and the estimated capacity is calculated. The estimation error for each model is then calculated for comparison. Capacity fade estimations for the Turnigy battery pack performed at different temperatures are shown in Tables 3.1, 3.2, 3.3 and 3.4. Estimated capacity is compared with the measured capacity for error calculation, where the measured capacity is the true capacity of the battery computed from each test.

From Figure 3.1 we can observe a significant drop in capacity after 20 test cycle sets for the battery at 0°C. Furthermore the battery seems to reach its EOL during the battery cycle after the 21st test. In contrast, the capacity of the battery at 10°C as shown in Figure 3.7 is observed to drop gradually after the 17th test and reaches EOL after the 20th test. The battery tested at 0°C is observed to perform better than the battery tested at 10°C. The estimation technique is able to estimate this as seen in Tables 3.1 and 3.2. Additionally Model 3 gives an accurate estimation of capacity as compared to other models and this is observed for 0°C and 10°C temperatures, shown in Tables 3.1c, 3.2c, respectively.

3.2.1 Temperature of 0°C

From the temperature range for a typical lithium ion battery we know that at 0°C the temperature falls below the recommended operating range. When the battery is charged/discharged at this temperature, the internal resistance of the battery rises to compensate for the lower

temperature thereby causing a rise in the battery temperature. The capacity fade in the battery is observed to be negligible until the end of the 16th aging test cycle.

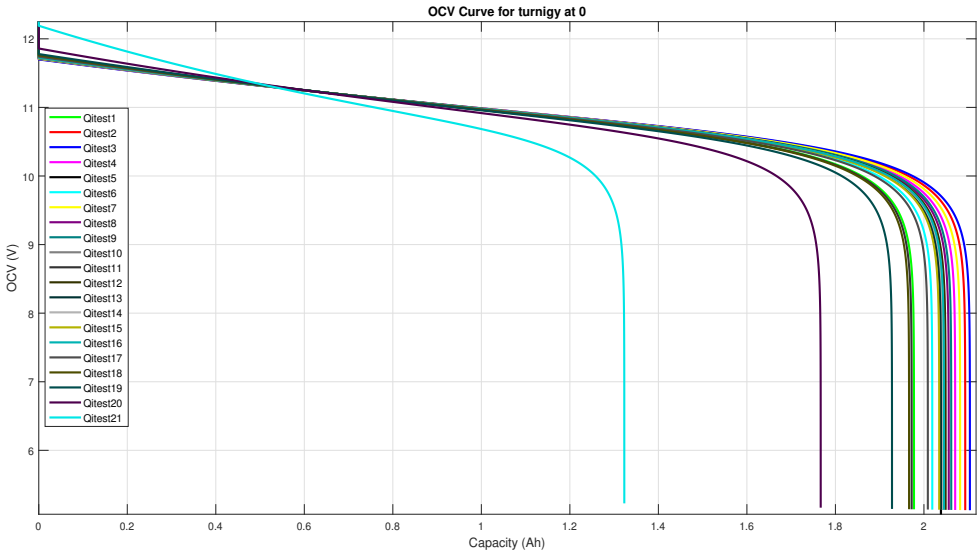

Figure 3.1: V-Q curve for Model 1 at 0°C

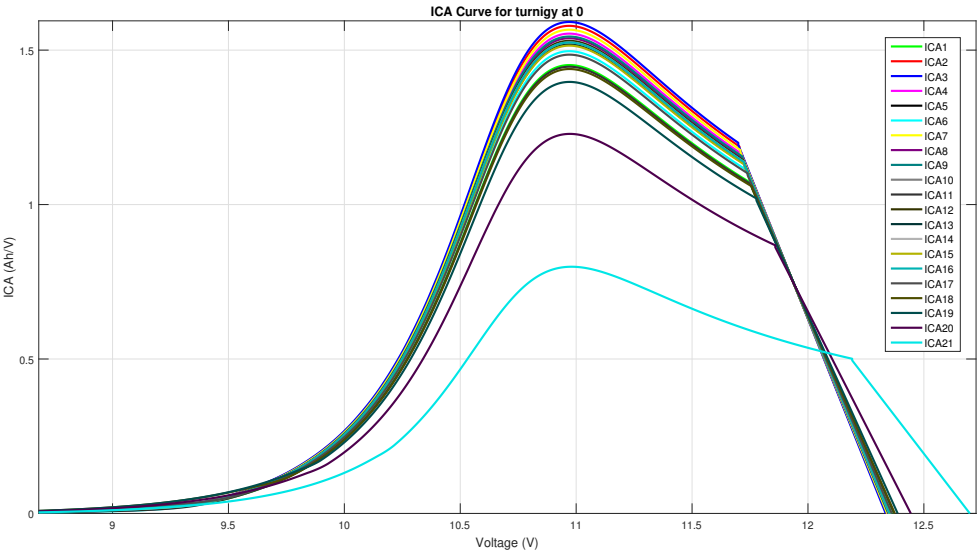

Figure 3.2: ICA curve for Model 1 at 0°C

The OCV curve and ICA curve using Model 2 are shown in Figure 3.3 and 3.4, respectively. The loss in battery capacity is seen to be notable after the 20th set of test cycle following which the battery reaches it EOL. This can be observed in the ICA curve.

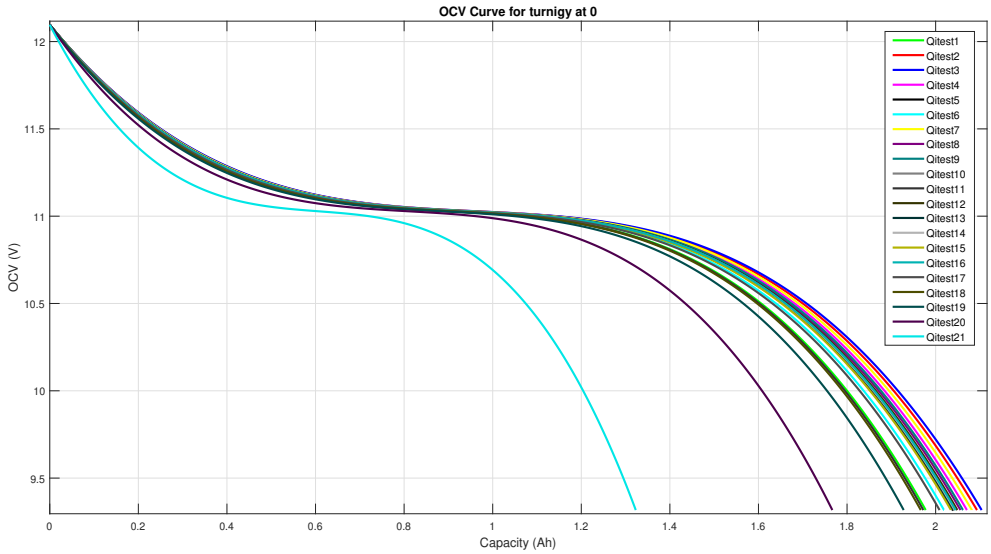

Figure 3.3: V-Q curve for Model 2 at 0°C

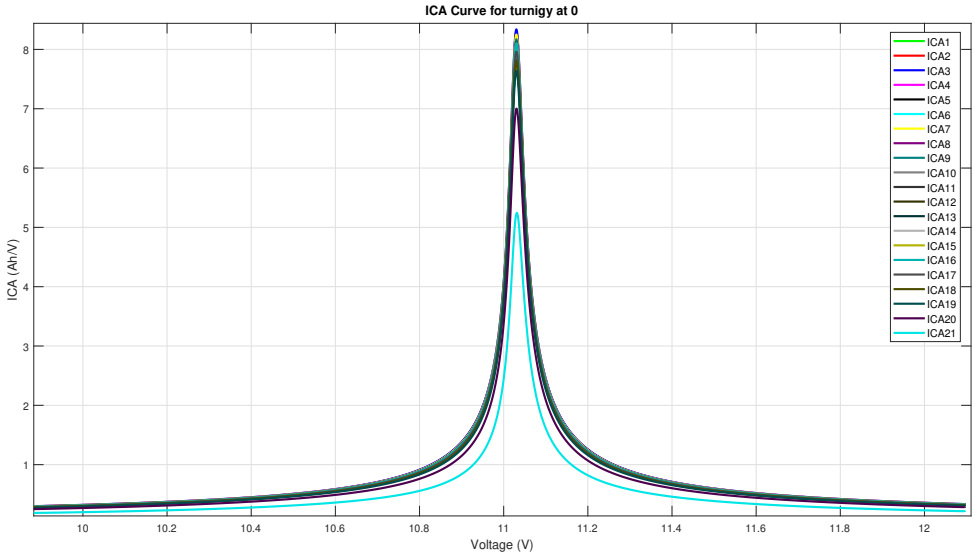

Figure 3.4: ICA curve for Model 2 at 0°C

The OCV curve and ICA curve using Model 3 are shown in Figure 3.5 and 3.6, respectively. The ICA curve tracks the degradation in the capacity after each test and displays the drop through the variation in the ICA peaks as the battery is cycled.

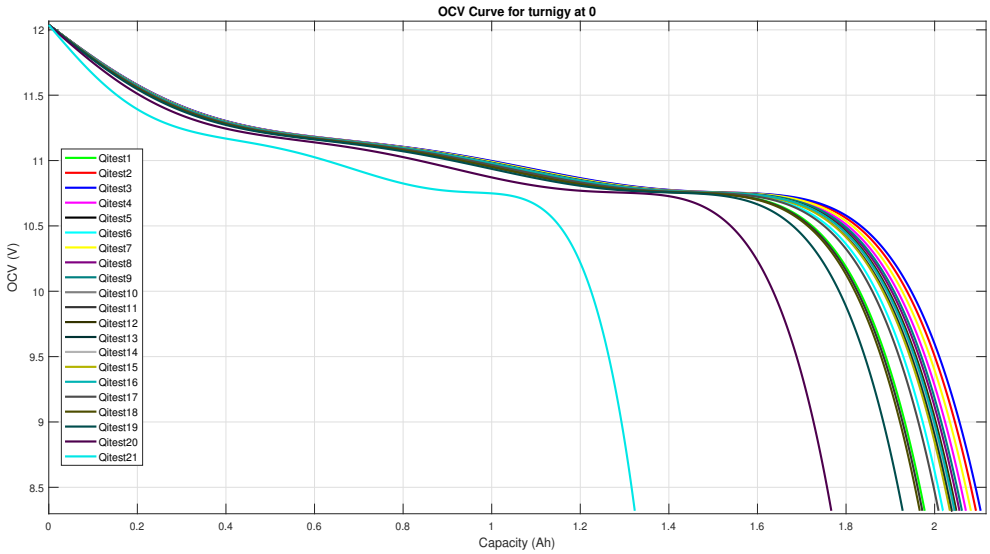

Figure 3.5: V-Q curve for Model 3 at 0°C

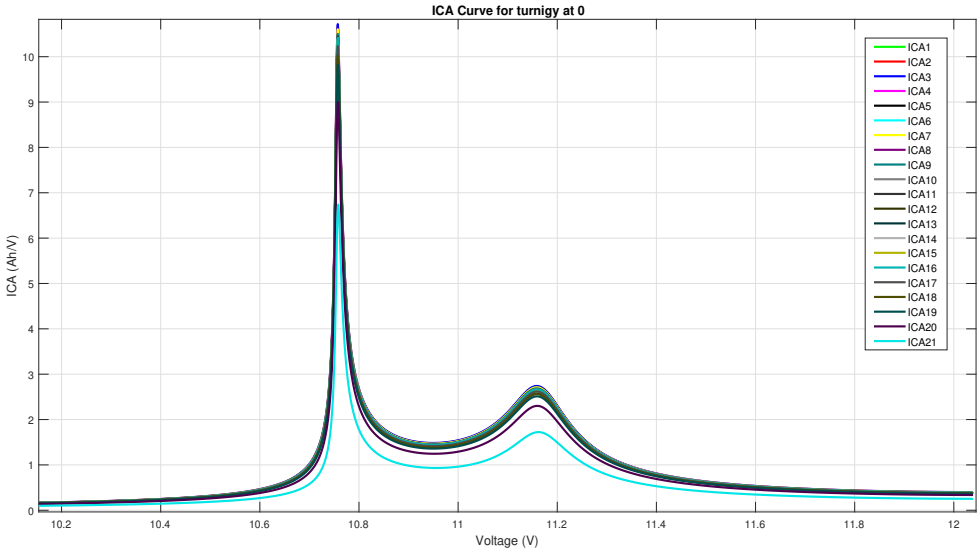

Figure 3.6: ICA curve for Model 3 at 0°C

Table 3.1 displays the calculation of estimated capacity for each OCV model.

Table 3.1: Capacity estimation calculation for 0°C

(a) **Capacity Estimation for Model 1**

Test	**Measured Capacity (Ah)**	**Estimated Capacity (Ah)**	**Error(%)**
Q_1test	1.9775	1.9774	.0040
Q_2test	2.0933	2.1181	1.1825
Q_3test	2.1039	2.1314	1.3051
Q_4test	2.0706	2.0893	0.9043
Q_5test	2.0385	2.0503	0.5783
Q_6test	2.0189	2.0251	0.3064
Q_7test	2.0818	2.1033	1.0345
Q_8test	2.0561	2.0720	0.7716
Q_9test	2.0617	2.0787	0.8228
Q_{10}test	2.0405	2.0531	0.6179
Q_{11}test	1.9722	1.9693	0.1468
Q_{12}test	2.049	2.0638	0.7209
Q_{13}test	2.0399	2.0524	0.6129
Q_{14}test	2.0433	2.0581	0.7258
Q_{15}test	2.0345	2.0477	0.6504
Q_{16}test	2.0453	2.0619	0.8126
Q_{17}test	2.0088	2.0195	0.5344
Q_{18}test	1.9664	1.9759	.48390
Q_{19}test	1.9279	1.9327	0.2508
Q_{20}test	1.7668	1.7416	1.4261
Q_{21}test	1.323	1.2497	5.5391

(b) **Capacity Estimation for Model 2**

Test	**Measured Capacity (Ah)**	**Estimated Capacity (Ah)**	**Error(%)**
Q_1test	1.9775	1.9744	0.1568
Q_2test	2.0933	2.09	0.1576
Q_3test	2.1039	2.1005	0.1616
Q_4test	2.0706	2.0672	0.1642
Q_5test	2.0385	2.0352	0.1619
Q_6test	2.0189	2.0157	0.1585
Q_7test	2.0818	2.0784	0.1633
Q_8test	2.0561	2.0527	0.1654
Q_9test	2.0617	2.0584	0.1601
Q_{10}test	2.0405	2.0372	0.1617
Q_{11}test	1.9722	1.969	0.1623
Q_{12}test	2.049	2.0458	0.1562
Q_{13}test	2.0399	2.0368	0.1520
Q_{14}test	2.0433	2.0399	0.1664
Q_{15}test	2.0345	2.0312	0.1622
Q_{16}test	2.0453	2.0421	0.1565
Q_{17}test	2.0088	2.0056	0.1593
Q_{18}test	1.9664	1.9639	0.1271
Q_{19}test	1.9279	1.9257	0.1141
Q_{20}test	1.7668	1.7648	0.1132
Q_{21}test	1.323	1.3231	0.0076

(c) **Capacity Estimation for Model 3**

Test	**Measured Capacity (Ah)**	**Estimated Capacity (Ah)**	**Error(%)**
Q_1test	1.9775	1.9774	0.0036
Q_2test	2.0933	2.0946	0.0599
Q_3test	2.1039	2.1053	0.0658
Q_4test	2.0706	2.0719	0.0630
Q_5test	2.0385	2.0397	0.0597
Q_6test	2.0189	2.02	0.0568
Q_7test	2.0818	2.0838	0.0973
Q_8test	2.0561	2.057	0.0439
Q_9test	2.0617	2.0621	0.0179
Q_{10}test	2.0405	2.0427	0.1077
Q_{11}test	1.9722	1.9715	0.0371
Q_{12}test	2.049	2.0507	0.0851
Q_{13}test	2.0399	2.0394	0.0236
Q_{14}test	2.0433	2.0439	0.0289
Q_{15}test	2.0345	2.0344	0.0072
Q_{16}test	2.0453	2.0463	0.0476
Q_{17}test	2.0088	2.0108	0.1
Q_{18}test	1.9664	1.9661	0.0151
Q_{19}test	1.9279	1.9280	0.0029
Q_{20}test	1.7668	1.7655	0.0719
Q_{21}test	1.323	1.3206	0.1836

3.2.2 Temperature at 10°C

The OCV and ICA curves for Model 1 are shown in Figure 3.7 and 3.8, respectively.

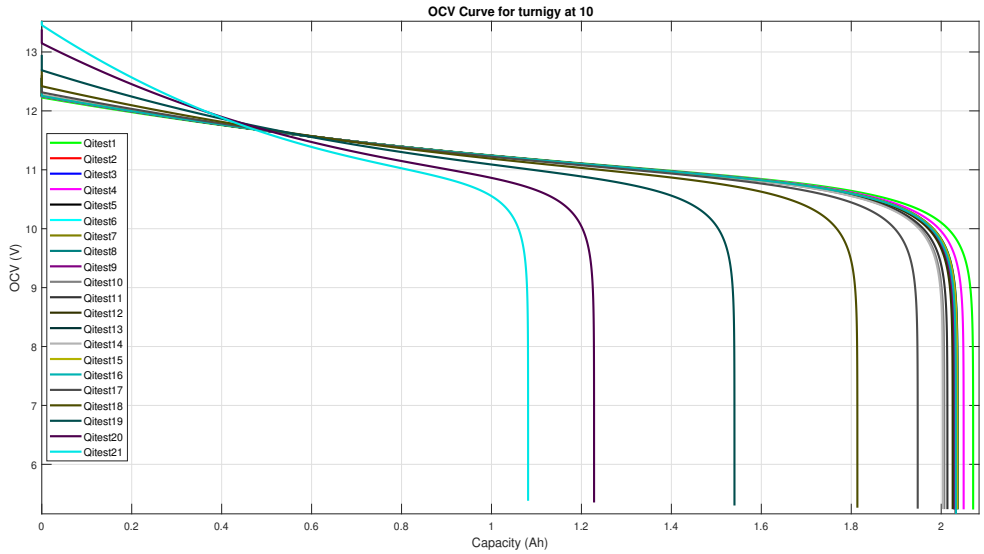

Figure 3.7: V-Q curve for Model 1 at 10°C

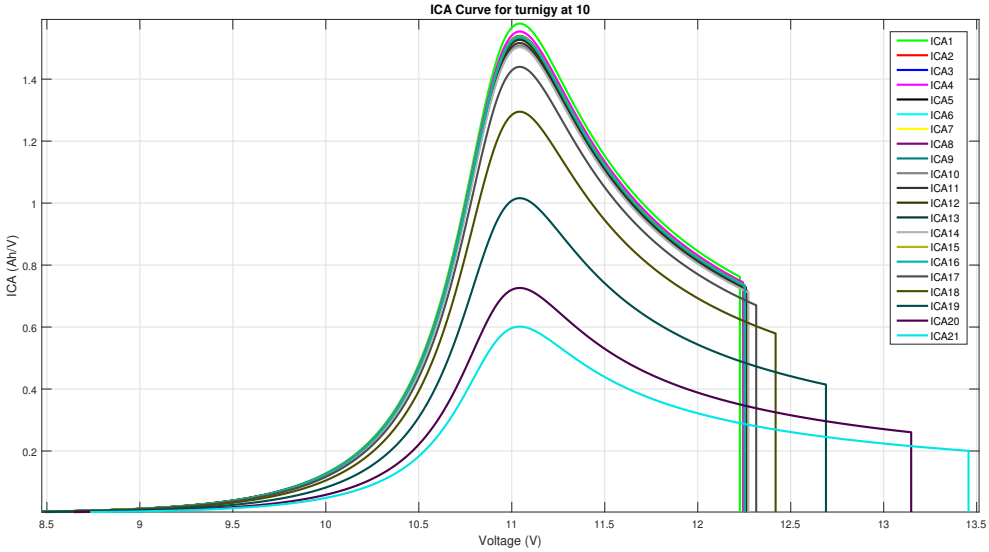

Figure 3.8: ICA curve for Model 1 at 10°C

The OCV and ICA curves for Model 2 are shown in Figure 3.9 and 3.10, respectively. The battery at 10°C shows a significant loss in the capacity from the 18th test and continues to lose its capacity at a higher rate until it reaches its EOL.

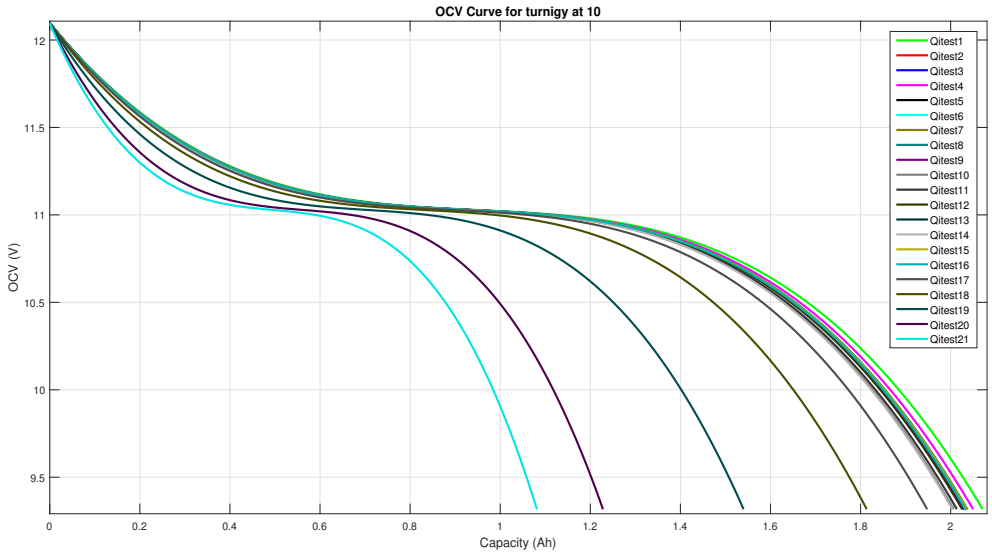

Figure 3.9: V-Q curve for Model 2 at 10°C

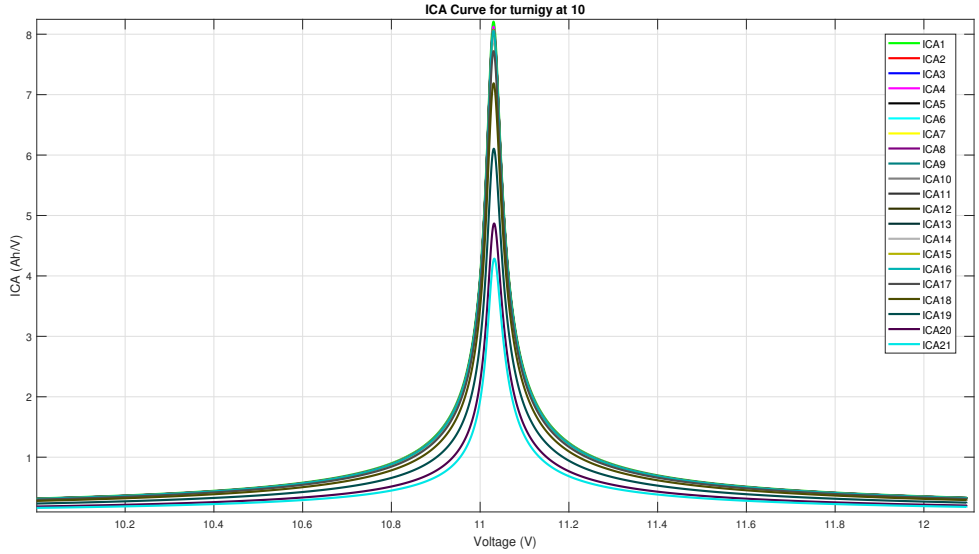

Figure 3.10: ICA curve for Model 2 at 10°C

The OCV and ICA curve for Model 3 are shown in Figure 3.11 and 3.12, respectively. Figures 3.8, 3.10 and 3.12 show that the battery at 10°C loses half of its total capacity, after 20 sets of aging cycles.

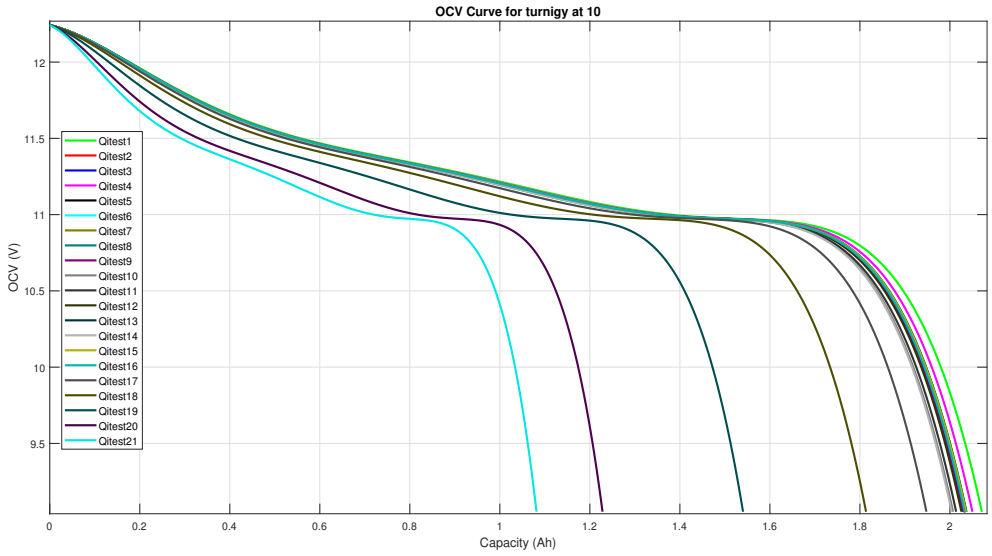

Figure 3.11: V-Q curve for Model 3 at 10°C

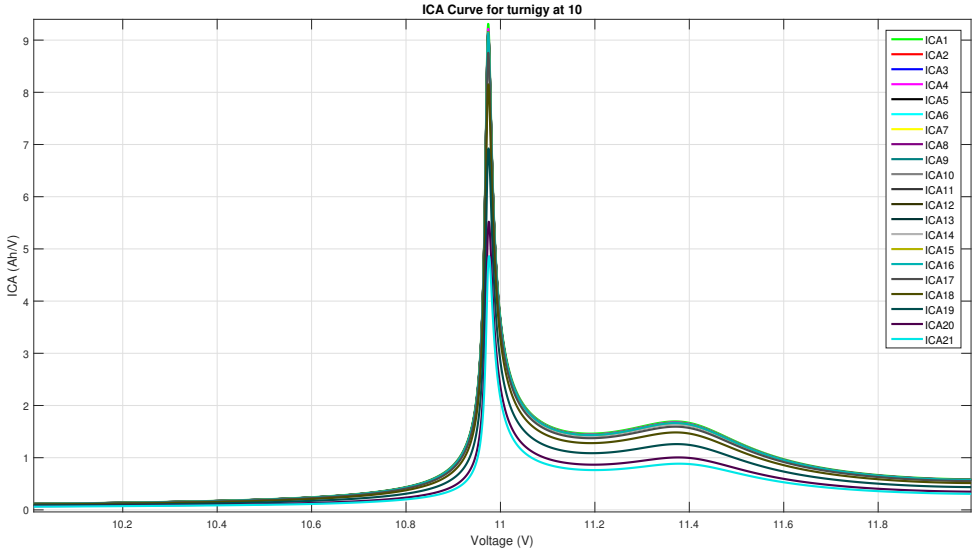

Figure 3.12: ICA curve for Model 3 at 10°C

Table 3.2 displays the calculation of estimated capacity for each OCV model.

Table 3.2: Capacity estimation calculation for 10°C

(a) **Capacity Estimation for Model 1**

Test	**Measured Capacity (Ah)**	**Estimated Capacity (Ah)**	**Error(%)**
Q_1test	2.071	2.071	0.0001
Q_2test	2.0323	2.029	0.1612
Q_3test	2.0309	2.0274	0.1739
Q_4test	2.0499	2.0476	0.111
Q_5test	2.0293	2.0252	0.2008
Q_6test	2.0365	2.0336	0.1424
Q_7test	2.0328	2.0299	0.1427
Q_8test	2.029	2.0268	0.1093
Q_9test	2.0294	2.0279	0.0762
Q_{10}test	2.0069	2.0039	0.1497
Q_{11}test	2.0138	2.0127	0.0565
Q_{12}test	2.0255	2.0268	0.0634
Q_{13}test	2.0367	2.0410	0.2112
Q_{14}test	2.0039	2.0067	0.1408
Q_{15}test	2.0359	2.047	0.5472
Q_{16}test	2.0326	2.0458	0.6482
Q_{17}test	1.9478	1.9534	0.285
Q_{18}test	1.8136	1.807	0.3653
Q_{19}test	1.5403	1.5223	1.1684
Q_{20}test	1.2281	1.2063	1.7773
Q_{21}test	1.0814	1.06	1.9796

(b) **Capacity Estimation for Model 2**

Test	**Measured Capacity (Ah)**	**Estimated Capacity (Ah)**	**Error(%)**
Q_1test	2.071	2.0694	0.0773
Q_2test	2.0323	2.0308	0.0738
Q_3test	2.0309	2.0295	0.0689
Q_4test	2.0499	2.0484	0.0732
Q_5test	2.0293	2.0278	0.0739
Q_6test	2.0365	2.035	0.0737
Q_7test	2.0328	2.0314	0.0689
Q_8test	2.029	2.0275	0.0739
Q_9test	2.0294	2.0278	0.0788
Q_{10}test	2.0069	2.0052	0.0847
Q_{11}test	2.0138	2.0124	0.0695
Q_{12}test	2.0255	2.0241	0.0691
Q_{13}test	2.0367	2.0353	0.0687
Q_{14}test	2.0039	2.0025	0.0699
Q_{15}test	2.0359	2.035	0.0442
Q_{16}test	2.0326	2.0316	0.0492
Q_{17}test	1.9478	1.9471	0.0359
Q_{18}test	1.8136	1.8132	0.0221
Q_{19}test	1.5403	1.5414	0.0714
Q_{20}test	1.2281	1.2316	0.285
Q_{21}test	1.0814	1.0861	0.4346

(c) **Capacity Estimation for Model 3**

Test	**Measured Capacity (Ah)**	**Estimated Capacity (Ah)**	**Error(%)**
Q_1test	2.071	2.071	0.0002
Q_2test	2.0323	2.0318	0.0223
Q_3test	2.0309	2.0307	0.0115
Q_4test	2.0499	2.0492	0.036
Q_5test	2.0293	2.0295	0.0092
Q_6test	2.0365	2.0370	0.0227
Q_7test	2.0328	2.0326	0.0082
Q_8test	2.029	2.0289	0.0052
Q_9test	2.0294	2.0289	0.0249
Q_{10}test	2.0069	2.0069	0.0021
Q_{11}test	2.0138	2.0143	0.0265
Q_{12}test	2.0255	2.0259	0.0219
Q_{13}test	2.0367	2.0364	0.0161
Q_{14}test	2.0039	2.0045	0.0297
Q_{15}test	2.0359	2.0360	0.0039
Q_{16}test	2.0326	2.0328	0.0114
Q_{17}test	1.9478	1.947	0.0391
Q_{18}test	1.8136	1.8134	0.0092
Q_{19}test	1.5403	1.5411	0.0521
Q_{20}test	1.2281	1.2302	0.1715
Q_{21}test	1.0814	1.0844	0.2774

3.2.3 Temperature at 25°C

The OCV and ICA curves for Model 1 are shown in Figure 3.13 and 3.14, respectively.

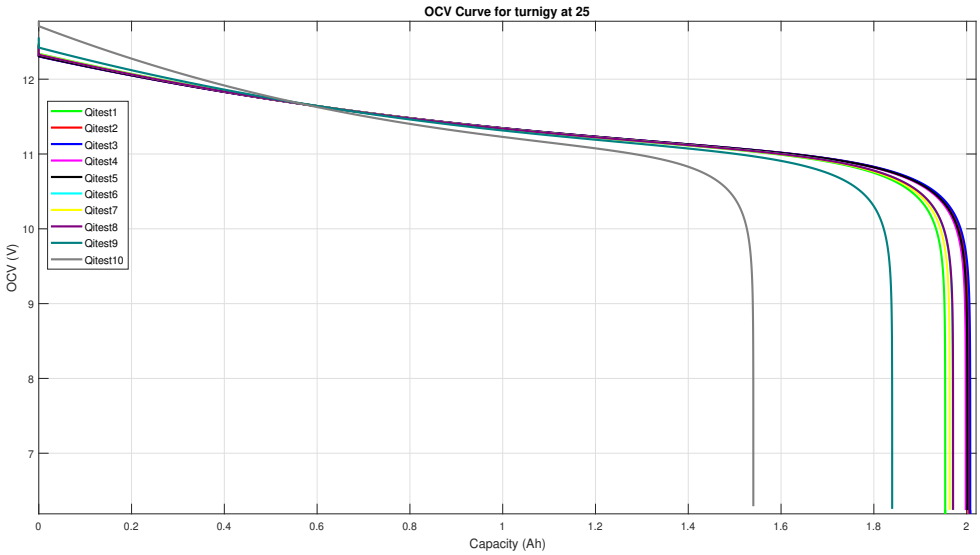

Figure 3.13: V-Q curve for Model 1 at 25°C

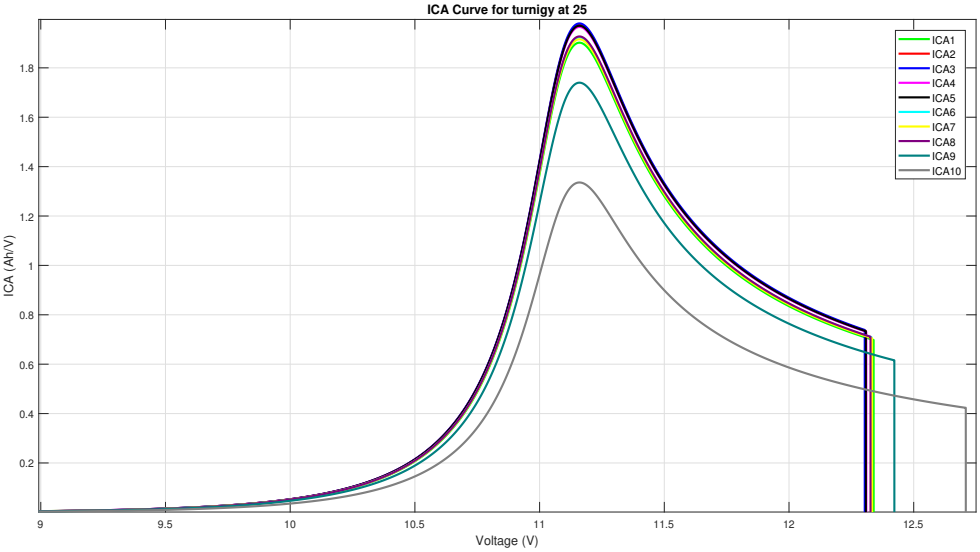

Figure 3.14: ICA curve for Model 1 at 25°C

The OCV and ICA curve for Model 2 are shown in Figure 3.15 and 3.16, respectively. The battery is observed to lose substantial capacity after the 9th test. The performance is lower at this temperature compared to 0°C and 10°C battery.

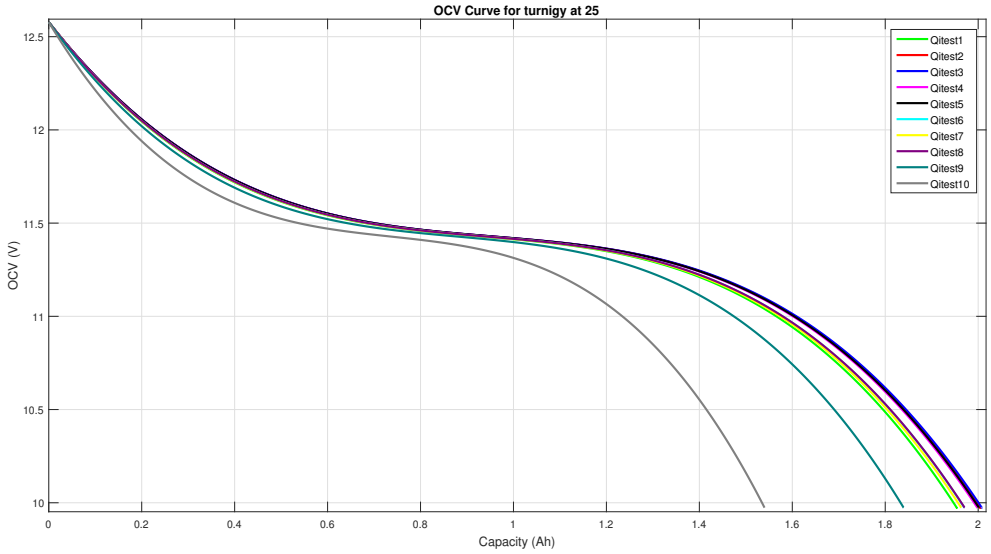

Figure 3.15: V-Q curve for Model 2 at 25°C

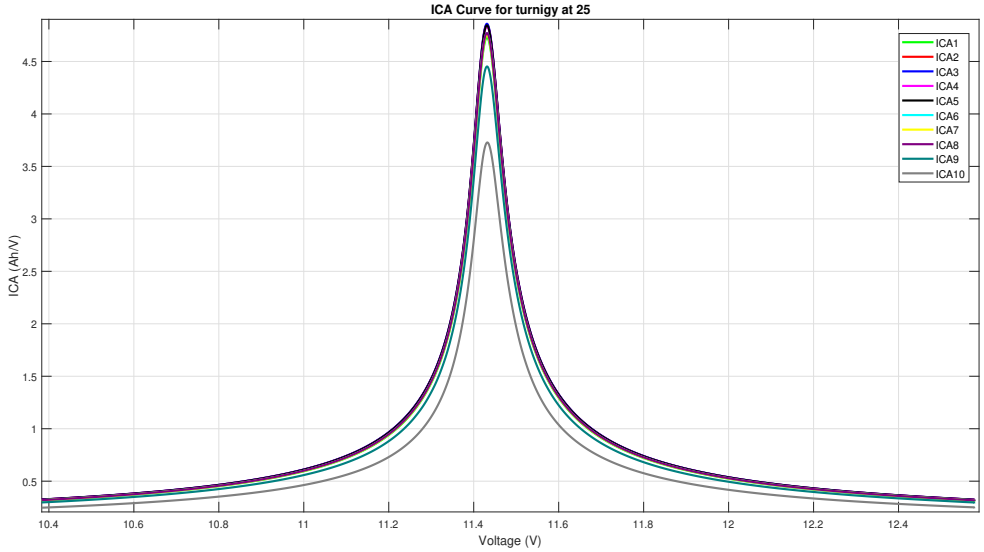

Figure 3.16: ICA curve for Model 2 at 25°C

The OCV and ICA curve for Model 3 are shown in Figure 3.17 and 3.18, respectively. At 25°C, the battery is unable to maintain the capacity for a longer duration. Low performance can be attributed to the cell chemistry of the lower grade battery.

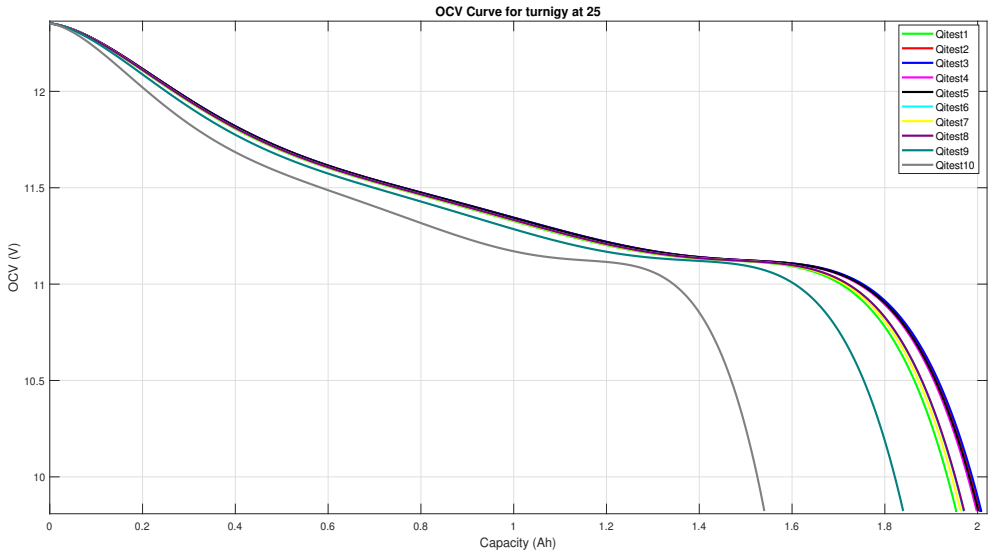

Figure 3.17: V-Q curve for Model 3 at 25°C

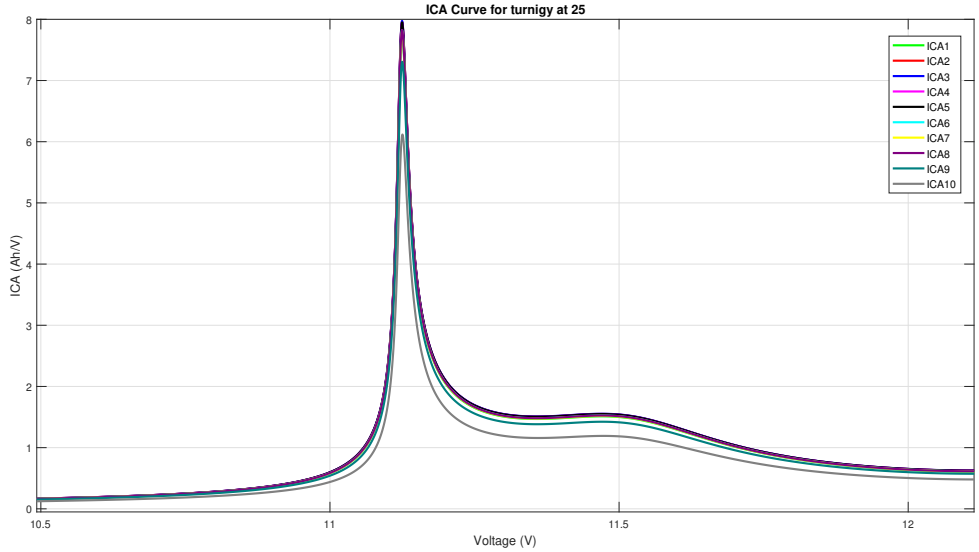

Figure 3.18: ICA curve for Model 3 at 25°C

Table 3.3 displays the calculation of estimated capacity for each OCV model.

Table 3.3: Capacity estimation calculation for 25°C

(a) **Capacity Estimation for Model 1**

Test	**Measured Capacity (Ah)**	**Estimated Capacity (Ah)**	**Error(%)**
Q_1test	1.9537	1.8896	3.281
Q_2test	2.0042	1.9413	3.1384
Q_3test	2.0076	1.9437	3.1829
Q_4test	1.998	1.9387	2.968
Q_5test	2.0014	1.9418	2.9779
Q_6test	1.9701	1.9103	3.0354
Q_7test	1.9634	1.9072	2.8624
Q_8test	1.9707	1.9185	2.6488
Q_9test	1.8393	1.7886	2.7565
Q_{10}test	1.5397	1.5038	2.3316

(b) **Capacity Estimation for Model 2**

Test	**Measured Capacity (Ah)**	**Estimated Capacity (Ah)**	**Error(%)**
Q_1test	1.9537	1.9465	0.3685
Q_2test	2.0042	2.0023	0.0948
Q_3test	2.0076	2.0062	0.0697
Q_4test	1.998	1.9964	0.0801
Q_5test	2.0014	1.9995	0.0949
Q_6test	1.9701	1.9682	0.0964
Q_7test	1.9634	1.9614	0.1019
Q_8test	1.9707	1.9688	0.0964
Q_9test	1.8393	1.8376	0.0924
Q_{10}test	1.5397	1.5389	0.052

(c) **Capacity Estimation for Model 3**

Test	**Measured Capacity (Ah)**	**Estimated Capacity (Ah)**	**Error(%)**
Q_1test	1.9537	1.9535	0.0102
Q_2test	2.0042	2.0031	0.0549
Q_3test	2.0076	2.0062	0.0697
Q_4test	1.998	1.9969	0.0551
Q_5test	2.0014	2.001	0.02
Q_6test	1.9701	1.9715	0.0711
Q_7test	1.9634	1.9639	0.0255
Q_8test	1.9707	1.9726	0.0964
Q_9test	1.8393	1.8391	0.0109
Q_{10}test	1.5397	1.5401	0.026

Model 1 displays inferior performance compared to other OCV models. The capacity estimation error shown in 3.3a is significantly higher than other models. While Model 2 shows a significant improvement in estimation of capacity, Model 3 gives the best estimate of capacity with estimation error of $<1\%$. In general, the polynomial models accurately estimate the capacity value for all the tests.

3.2.4 Temperature at 50°C

The OCV and ICA curves for Model 1 are shown in Figure 3.19 and 3.20, respectively.

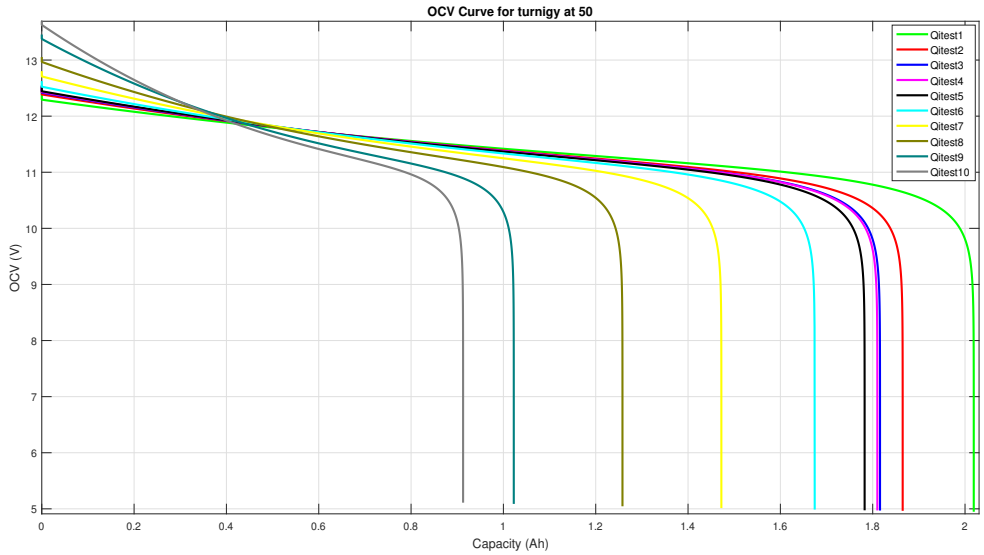

Figure 3.19: V-Q curve for Model 1 at 50°C

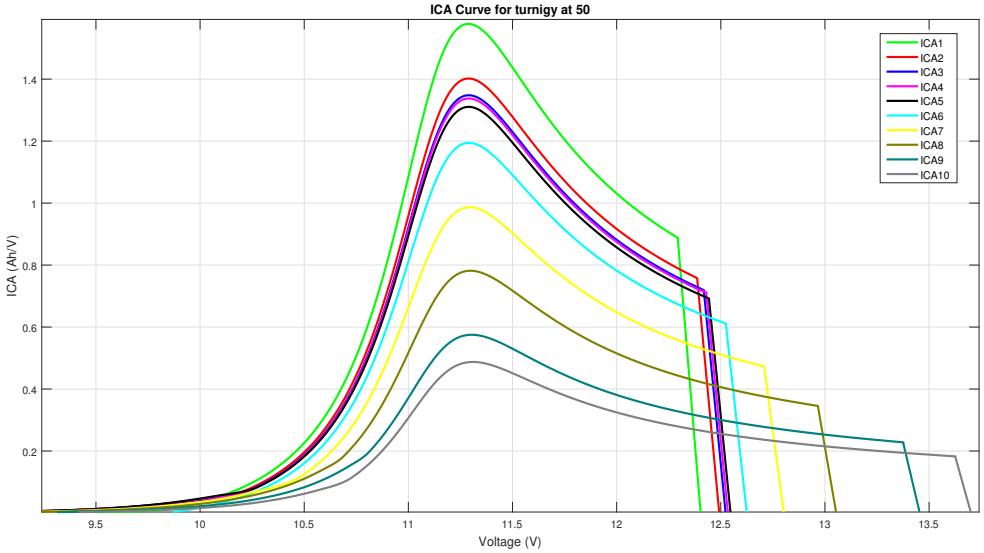

Figure 3.20: ICA curve for Model 1 at 50°C

The OCV and ICA curves for Model 2 are shown in Figure 3.21 and 3.22, respectively. As expected the battery at 50°C shows a degraded performance due to the high temperature.

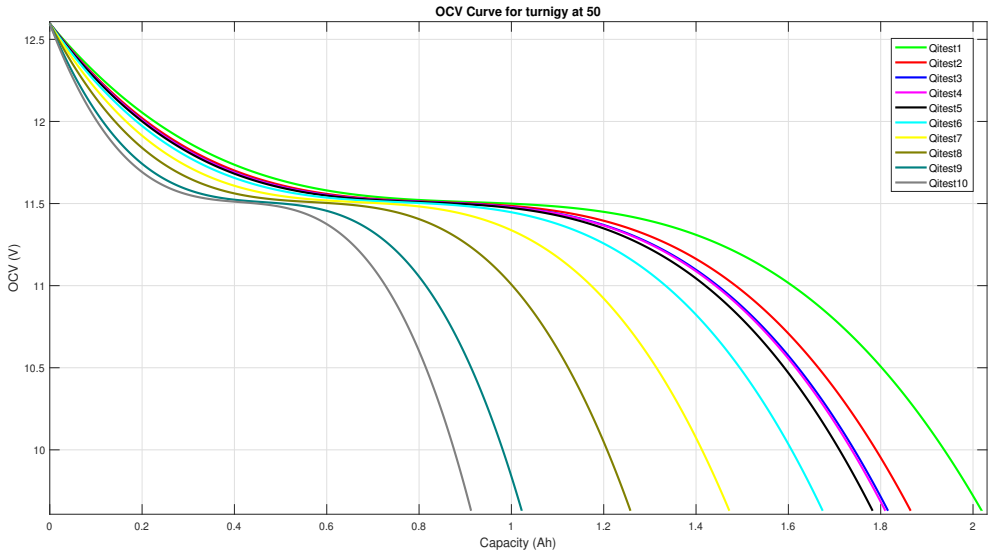

Figure 3.21: V-Q curve for Model 2 at 50°C

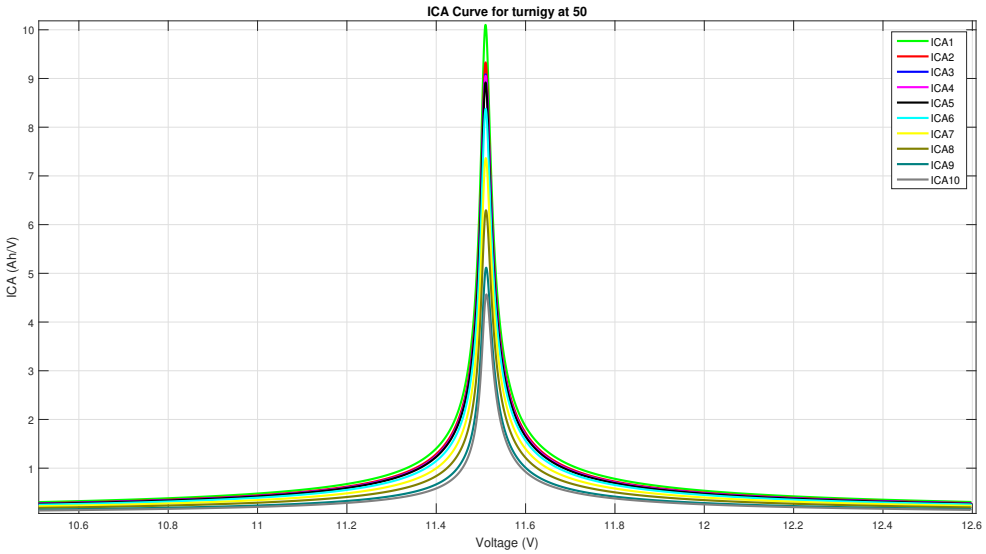

Figure 3.22: ICA curve for Model 2 at 50°C

The OCV and ICA curves for Model 3 are shown in Figure 3.21 and 3.22, respectively. The capacity degrades faster at this temperature and thus a substantial drop after each test can be observed.

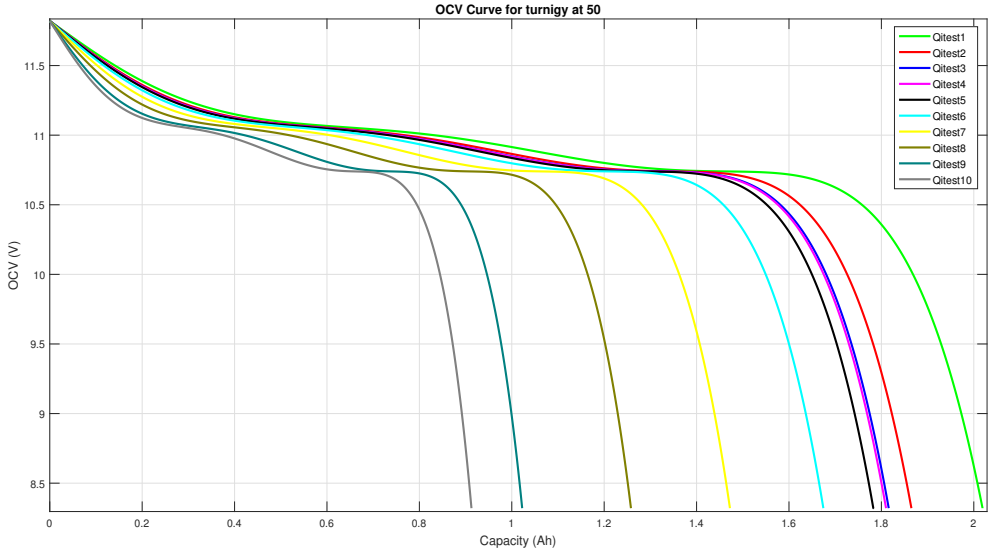

Figure 3.23: V-Q curve for Model 3 at 50°C

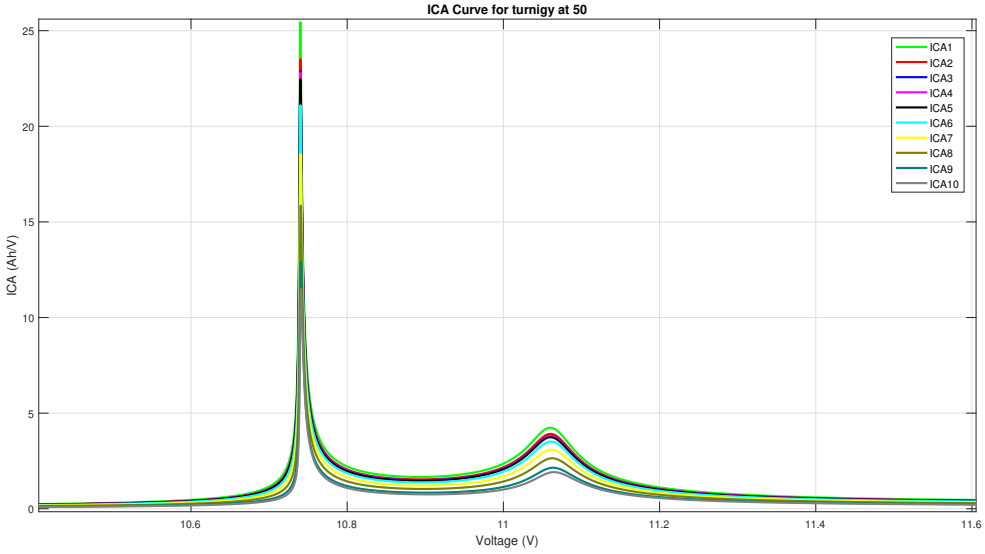

Figure 3.24: ICA curve for Model 3 at 50°C

Table 3.4: Capacity estimation calculation for 50°C

(a) **Capacity Estimation for Model 1**

Test	**Measured Capacity (Ah)**	**Estimated Capacity (Ah)**	**Error(%)**
Q_1test	2.0189	2.005	0.6885
Q_2test	1.865	1.8575	0.4021
Q_3test	1.8159	1.8075	0.4626
Q_4test	1.8101	1.8024	0.4254
Q_5test	1.7825	1.7773	0.2917
Q_6test	1.6744	1.6459	1.7021
Q_7test	1.4722	1.4603	0.8083
Q_8test	1.258	1.2487	0.7393
Q_9test	1.0225	1.0156	0.6748
Q_{10}test	0.9127	0.8994	1.4572

(b) **Capacity Estimation for Model 2**

Test	**Measured Capacity (Ah)**	**Estimated Capacity (Ah)**	**Error(%)**
Q_1test	2.0189	2.0162	0.1337
Q_2test	1.865	1.8629	0.1126
Q_3test	1.8159	1.8139	0.1101
Q_4test	1.8101	1.8082	0.1050
Q_5test	1.7825	1.7808	0.0954
Q_6test	1.6744	1.6575	1.0093
Q_7test	1.4722	1.4719	0.0204
Q_8test	1.258	1.2592	0.0954
Q_9test	1.0225	1.0253	0.2738
Q_{10}test	0.9127	0.9158	0.3397

(c) **Capacity Estimation for Model 3**

Test	**Measured Capacity (Ah)**	**Estimated Capacity (Ah)**	**Error(%)**
Q_1test	2.0189	2.0189	0.0001
Q_2test	1.865	1.8617	0.1757
Q_3test	1.8159	1.8102	0.3120
Q_4test	1.8101	1.8057	0.2421
Q_5test	1.7825	1.7786	0.2177
Q_6test	1.6744	1.6655	0.5328
Q_7test	1.4722	1.4618	0.7076
Q_8test	1.258	1.2509	0.5676
Q_9test	1.0225	1.0180	0.4370
Q_{10}test	0.9127	0.9040	0.9545

Table 3.4 displays the calculation of estimated capacity for each OCV model. Capacity estimated by Model 1 is the least accurate. This seems obvious as the OCV model was unable to estimate the OCV-SOC curve accurately as discussed earlier. The polynomial OCV models were more accurate in estimating the capacity considering the nature of the polynomial equations. However, as seen from Tables 3.4b and 3.4c, Model 3 could not estimate the capacity accurately, as it was seen for other temperatures, due to over-fitting of the test data affecting the calculation of capacity. Model 2, however, estimated capacity fade in the battery pack accurately with relatively less estimation error compared to Model 3.

3.3 ICA Calculations

The IC analysis of the ICA curve is concluded with the calculation of the capacity accumulated by the peaks. The capacity is calculated by taking the integration of the area under the curve. The integration is done using the MATLAB command *trapz*, which is a trapezoidal method for numerical integration. Since the results obtained from Model 1 and Model 2 form single peaks over the entire voltage range, the area under the curve is taken for the entire voltage range occupied by the peak. For Model 3, we have two peaks corresponding to the plateaus in the OCV curve. The calculation of the capacity is done under the peak formed at higher voltage. The voltage range is generally represented by the minimum points at either ends of the peak.

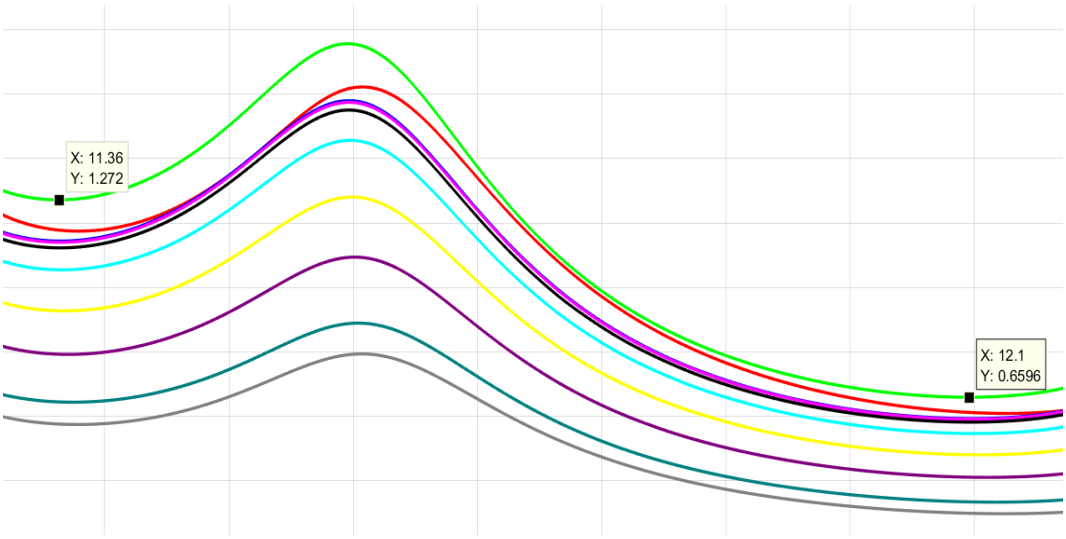

Figure 3.25: Voltage range for area integration

The area calculated for Model 3 is calibrated for the final capacity estimation. The calibration is done by taking a ratio of the area calculated with respect to the initial measured capacity, where measured capacity is the true capacity calculated from the test data. The ratio is used as the calibration factor to estimate the capacity. The error is calculated by taking the difference between estimated and measured capacity.

Figure 3.25 shows the region where the area calculation is performed. The trapezoidal method for the ICA curve as shown in Figure 3.25 can be approximated with,

$$\frac{b-a}{2N}\sum_{n=1}^{N}(IC_n + IC_{n+1}) \tag{3.1}$$

where, a and b are the minimum voltage points for the peak curve under which the summation is performed, N is the number of data points between a and b and IC_n are the IC points computed in Equation 2.1 summed over each time period.

The capacity accumulated over the area is calculated for all the $Q_i$tests. The calculated capacity is scaled when required, to achieve the true estimated capacity.

Thus, it can be concluded that the error in capacity estimation using the combined model is considerably higher than the polynomial equation models. This is because the combined model does not capture the nonlinear characteristics of OCV-SOC curve as well as the polynomial equation.

3.4 Implementation of ICA on mRPT test data

The test data from $Q_i$tests consists of a large set of data and takes longer time to run which is not practical to implement during a normal operation. Therefore, it is highly desirable to have testing data that can accurately predict the capacity fade in a battery pack or a cell, as accurately as the test data from $Q_i$test, only with considerably less data points. The idea is to use mRPT data with less data points and predict the capacity fade using the OCV model and IC analysis technique.

The mRPT consists of voltage discharge at a high C rate followed by a rest period. During the rest period the voltage value is observed to rise gradually to its OCV value and then settle after a certain period of time. The OCV value at the end of each rest period is taken as the true OCV value at the SOC level. Each pulse causes a drop in the SOC by 10% and the mRPT test is conducted until the SOC drops to 50% of its initial value. The OCV

values and corresponding SOC values are extracted from each mRPT data set. Thus, in all, a set of 6 data points for the OCV and SOC are extracted as shown in Figure 3.26. This set of data points is used for the estimation of OCV-SOC curve using a nonlinear OCV model equation. Since there are only 6 data points for an accurate OCV curve estimation, it is a challenge to find a suitable equation that can fit a curve to the limited number of points.

For this thesis, an initial OCV model equation is chosen that is nonlinear in the parameters. The OCV-SOC curve is derived from the curve-fit toolbox in MATLAB. The required voltage data is then generated using the SOC values calculated from the current data points without the rest phase. The SOC data is obtained using the coulomb counting method and the data ranges from 100%-50%. The SOC data for each mRPT test is used with the curvefit model to generate the OCV data points. Additionally, charge accumulation for each time step, over the entire test data, produces the capacity data points. These calculated capacity and OCV values are then used for the IC analysis from ICA curves.

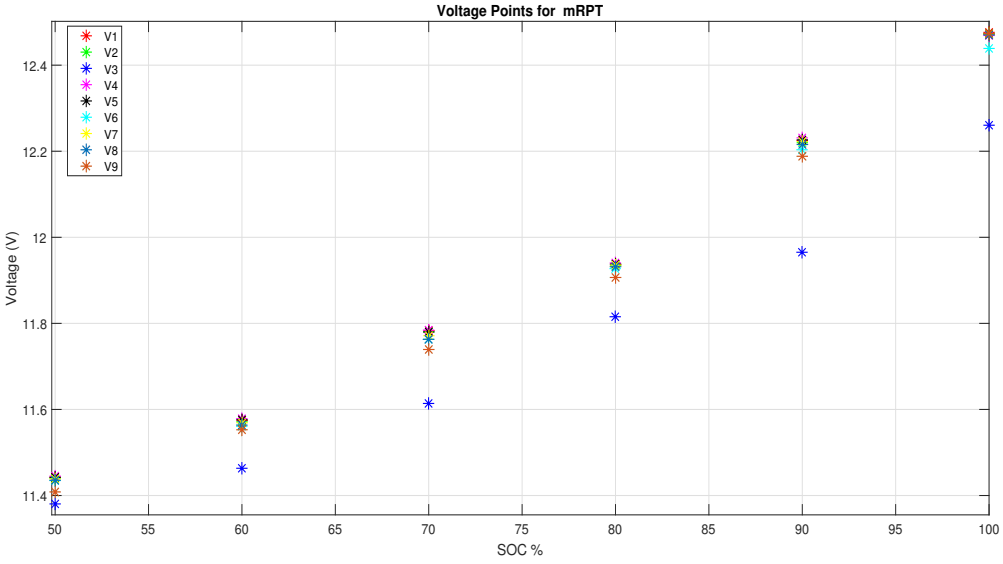

Figure 3.26: Voltage Points from mRPT test

The OCV model equation for the mRPT test data is shown as follows,

$$OCV Model : a + bx + cx^2 + dx^3 + e^{-(\frac{x}{x-a1})^3} \tag{3.2}$$

where a, b, c, d are linear parameters, $a1$ is the non-linear parameter, and x represents SOC values. Non-linear least squares is used for the parameter estimation. The OCV points estimated are then used for generating OCV data points. The voltage points extracted from the mRPT data for all the tests are shown in Figure 3.26. The drop in the voltage value can be observed in the figure. This drop in the voltage can be attributed to the loss in the battery capacity. However, due to the testing procedure followed for the mRPT, the voltage variation is quite low, this is explained next.

3.5 Capacity Estimation for mRPT data

Estimation of capacity using $Q_i$test is considerably easier due to the number of data points available to predict and estimate the capacity from the OCV models, provided that a good OCV model is established. With mRPT data, the extraction of the OCV-SOC data points for the SOC ranging only from 100% - 50% limits the available data for OCV estimation. Therefore, it is logical to use an OCV model that is nonlinear in the parameters. The OCV model used for this thesis is given in Equation 3.2. The OCV-SOC curve produced from the curvefit is shown in Figure 3.27. From the figure, it is observed that the OCV curve has a slight flat region around 12V and 11.6V. As compared to a full capacity test, that is from 100% to 0% SOC, the plateau corresponds to the initial transition stage during the discharging of the battery. This plateau translates to a distinct ICA peak shown in Figure 3.28.

The ICA curve from the mRPT data does not show the capacity loss observed in the battery pack. This is due to the testing profile used for the cycling of the battery pack. The mRPT test is executed at constant current mode where each pulse is applied for the time

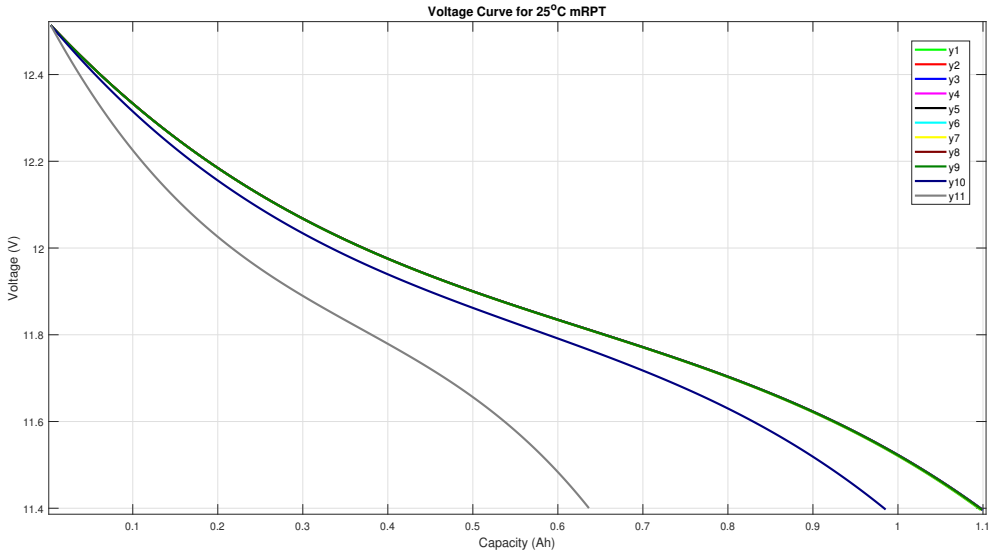

Figure 3.27: OCV curve for nonlinear polynomial model

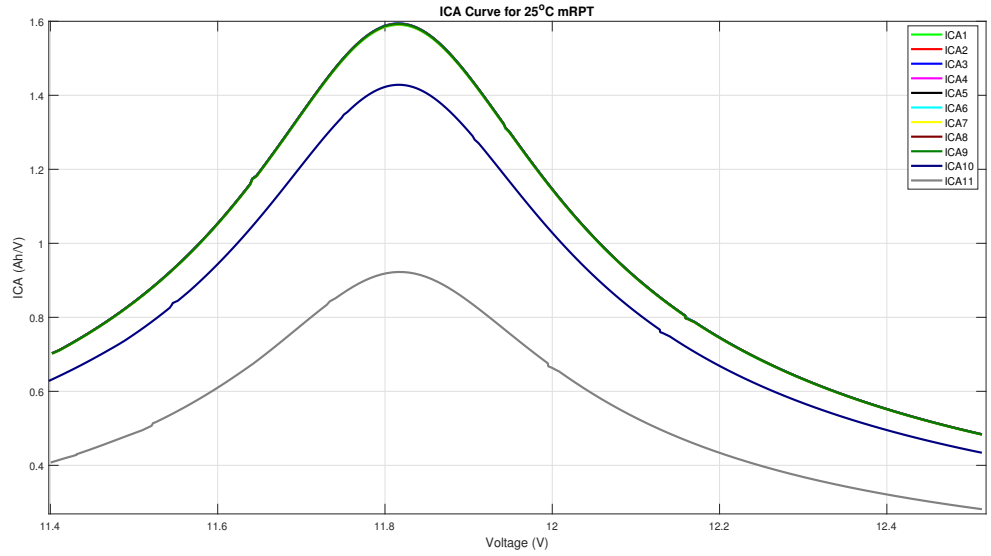

Figure 3.28: ICA curve for nonlinear polynomial model

taken to discharge the battery pack by 10% SOC. However, as the battery loses its capacity, the C rate for the battery changes. Therefore, if the change for the capacity is not accounted for, the charge accumulation for the test will remain the same. The testing profile for mRPT

was executed without accounting for this change in capacity. Hence, the test results have been observed to be erroneous and not fit for the estimation of capacity fade in the battery pack.

3.6 Summary

In this chapter, we have implemented the OCV model for OCV-SOC curve estimation using the Q_i test data. The IC analysis for capacity fade estimation was performed for the test data. The results of the calculation showed accurate estimation of the capacity fade using the Q_i test data. The estimation technique was implemented on mRPT data to explore the advantage of having lesser data points compared to a Q_i test. However, the calculation for the IC analysis exhibited no capacity fade in the ICA curve. Therefore, it is concluded that the poor estimation using mRPT test data is due to deficiencies in the testing procedure. Varying the time for each pulse in the mRPT or updating the C rate would account for the capacity fade thereby giving accurate IC analysis.

The next chapter will explore this methodologies for an automotive grade battery cell by LG Chem. In the testing and data collection for this battery, the capacity fade was accounted for in the data collection. The testing data from the cell is analyzed for the IC analysis in the similar process. The capacity fade estimation is implemented on the characterization test and the pulse test of the LG Chem cell and the results are presented.

CHAPTER 4

LG CHEM BATTERY

4.1 Introduction

In the previous chapter, we discussed the estimation of capacity for a lower grade Turnigy battery pack used for small scale applications. This chapter presents the testing profiles and capacity fade of a better grade battery - LG chem single cell with a capacity of 15 Ah, used for industrial applications. Typically an automotive grade cell has a life span of over 10 years. The cell capacity is observed to drop insignificantly over this period, thus, making them a great source of power to run a vehicle. The battery considered in this experiment is of lithium-ion type made by LG Chem. The data for the battery used for this thesis was obtained from CAR-OSU laboratory in Ohio. This chapter discusses the series of test profiles implemented on the battery at each period, followed by an analysis of the data for capacity fade over the entire duration of tests conducted. This chapter later addresses the estimation of capacity fade for a reduced amount of data using the estimation methods mentioned in previous chapters.

4.2 Testing Profiles

The testing profile sets for the LG Chem cell is different from the Turnigy battery pack. The LG Chem cell undergoes 3 different test sets namely, aging cycle, capacity test followed by HPPC test. The LG Chem cell is a high capacity automotive grade cell, so the cell must undergo extensive aging cycles to obtain any noticeable change in the capacity. The aging cycle is a set of charge sustaining(CS) and charge depleting(CD) cycles followed by a charging cycle to its maximum voltage. Each cycle is executed at high C rates. then the cell is characterized by executing the capacity test and a HPPC test. The capacity test is a full discharge and a full charge of the cell at 1C rate. This is the same as the Q_i test run for

the Turnigy battery pack. The HPPC test as explained earlier is a set of pulses executed at 10% DOD increments to reach the SOC range with rest periods. The testing profile will be explained further in detail.

4.2.1 Aging Cycle

The aging cycle is conducted on the LG Chem cell to replicate the working of a battery in PHEVs. (Cordoba-Arenas et al., 2015) describes the process of the CS-CD in the aging cycle. Figure 4.1 shows a single cycle of the the aging cycle set.

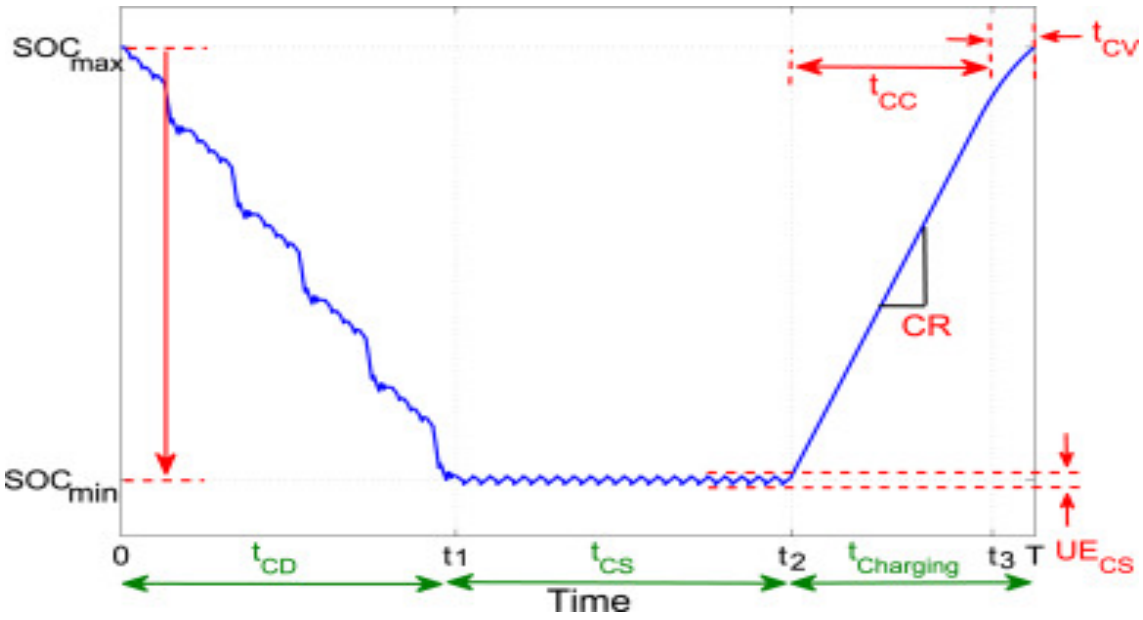

Figure 4.1: CD-CS curve for LG Chem cell. Figure from (Cordoba-Arenas et al., 2015)

During the CD mode the cell is operated in pure electric mode (where all of the power is delivered to the electric motor from the battery), or hybrid mode (where the vehicle power is delivered from the battery or/and the ICE). The net decrease in the battery SOC is allowed to drop from the maximum SOC to a minimum SOC value. During the CS mode the vehicle operates strictly in hybrid mode. In this mode, the battery is operated at a constant SOC value. The SOC value in CS mode varies within a range defined by UE_{CS} with average

value of SOC_{min} as shown in Figure 4.1. The aging cycle is executed at different mode configurations. The cycle consists of only CD mode at different SOC_{min} values and different C rates for each SOC_{min} value, only CS mode with similar combination of SOC_{min} and C rates and a mixed operation that is based on the time for which a CS mode or a CD mode is allowed to be executed. The time for the mixed operation is based on a ratio of t_{CD} and (t_{CD}+t_{CS}). The CD and CS mode are followed by a constant charge in CC-CV mode of operation. In the CC mode the battery charges with constant current value. When the cell reaches its maximum voltage the charging continues in constant voltage mode until the current reduces to a minimum value.

4.2.2 Capacity test

The capacity test performed in the LG Chem cell is the same as Q_i test performed for the Turnigy battery pack. The cell is charged and discharged in CC-CV mode. The charging/discharging is done in CC mode at 1C rate, which is 15A since the battery capacity is 15Ah. As the cell voltage reaches the max/min value depending on the charge/discharge process, the test continues in CV mode until a minimum current value is attained.

4.2.3 HPPC Test

The capacity test is followed by a HPPC test. The test is conducted at 2C rate, that is, 30A current. As the name suggests, the test is performed with discharge pulse followed by a rest period. The discharge pulse is designed to drop the SOC by 10% DOD decrements and a rest period of 1 hour before the next pulse is executed. A discharge and regeneration pulse with current of 5C(75A) and 3.75C(56.25A) respectively, are applied prior to each pulse. The HPPC pulse discharges the cell from 100% to 0% SOC with 10% DOD decrements. The cell is then charged to the maximum voltage limit in CC-CV mode. Each set of capacity and HPPC tests are performed after approximately two weeks of aging cycles to evaluate the capacity loss.

4.3 Implementation of ICA on Capacity Test

The previous chapter discussed the effect of aging cycle in a battery pack consisting of 3 cells connected in series. Furthermore, the battery pack used for the aging test is of lower grade used for small scale applications. The battery was aged to its EOL in the span of few months. However, the LG Chem cell used for aging tests is of a higher quality used in electric vehicle battery packs. The cell underwent a series of aging cycles for several weeks before every capacity test. The LG Chem cell capacity shows notable change after several sets of aging cycles that are designed to degrade the cell capacity until its EOL.

Each capacity test performed shows the variation in the cell capacity as it depletes. The LG Chem cell testing was performed at a single temperature of 30°C. Similar to the Turnigy battery pack, the capacity test data is used to derive the OCV-SOC curve using the OCV models- Model 1, Model 2 and Model 3, given in Table 2.1. OCV-SOC data points are estimated using least squares similar to the Turnigy battery pack. Capacity data points are computed using the accumulation of charge over the entire duration of the test. Thereafter, the ratio of increments of capacity and OCV data are evaluated to produce ICA curves. The following section shows the OCV curves and their respective ICA curves for the analysis of capacity fade observed in the cell.

4.4 Capacity Estimation Using Full Data Sets

A capacity test for the LG Chem cell consists of 7 test data sets. Each test is performed to evaluate the capacity degradation in the cell after running the aging cycles for several weeks. The IC analysis on the capacity fade is performed using the OCV models and the ICA peak tracking method. Estimation of capacity fade using each model is evaluated and the results are discussed.

The OCV curve and ICA plot for Model 1 are shown in Figure 4.2 and 4.3, respectively. The OCV curve for Model 1 does not capture the transitions in the cell which leads the ICA curve to terminate before the curve is completed.

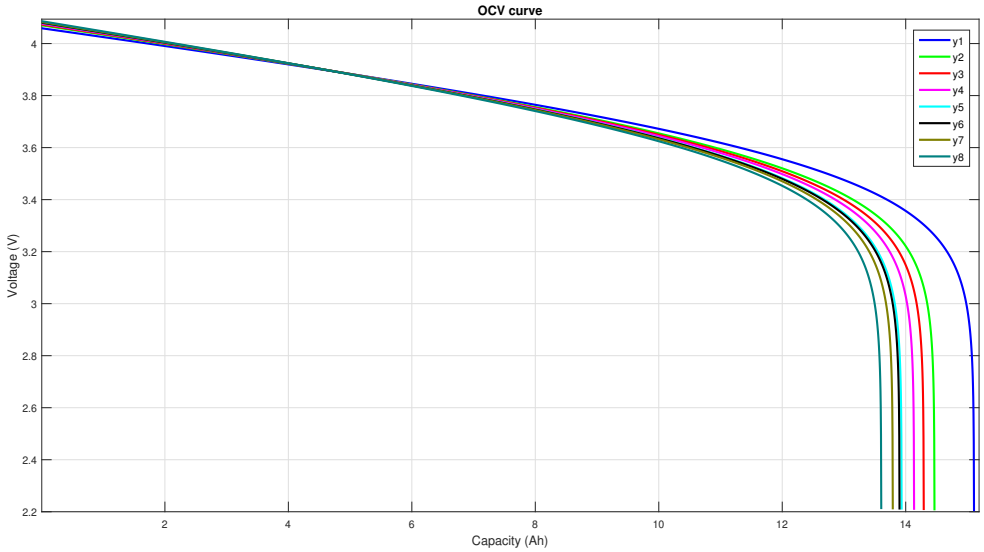

Figure 4.2: OCV curve for Model 1

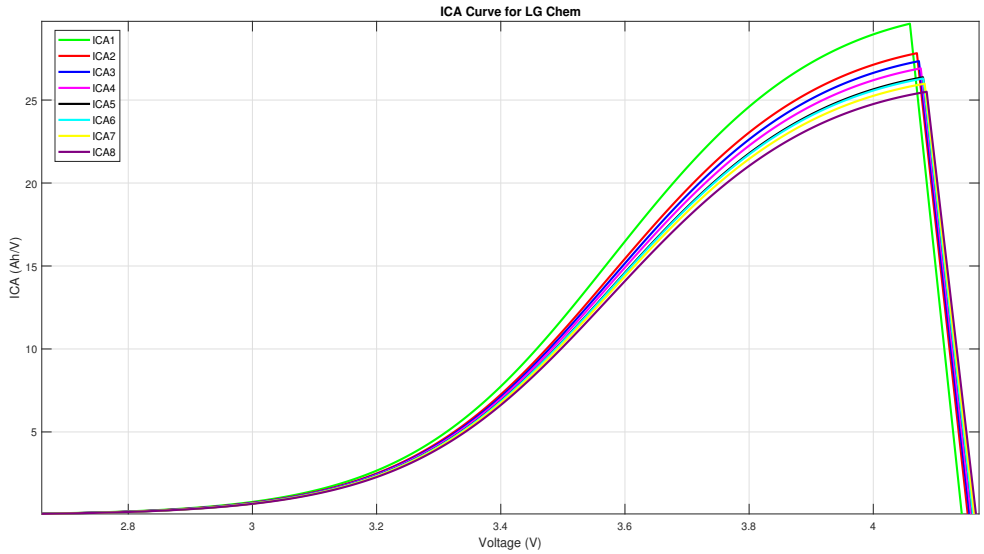

Figure 4.3: ICA curve for Model 1

The OCV curve and ICA plot for Model 2 are shown in Figure 4.4 and 4.5, respectively. Variation in the OCV curve shows the gradual decrease in the cell capacity, however the change in the capacity is not significantly high.

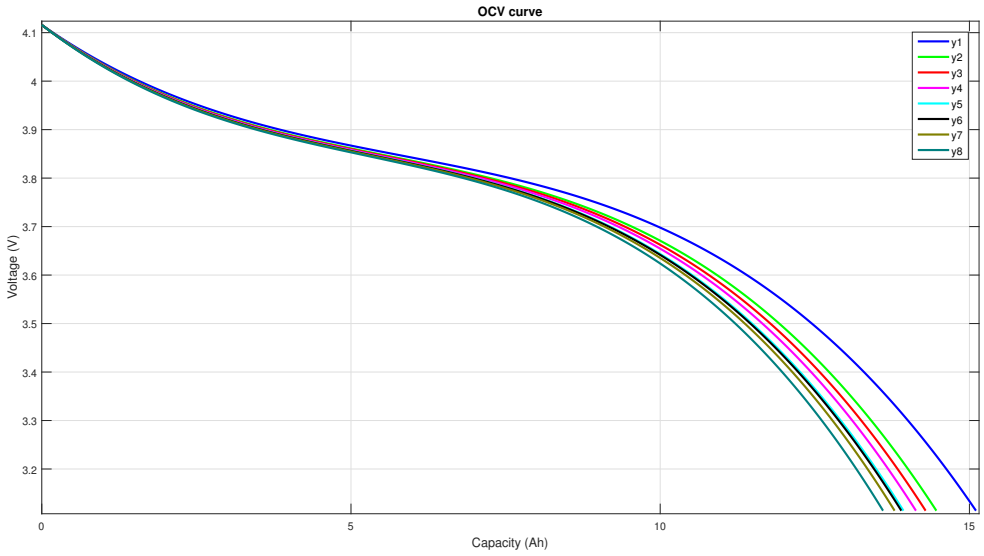

Figure 4.4: OCV curve for Model 2

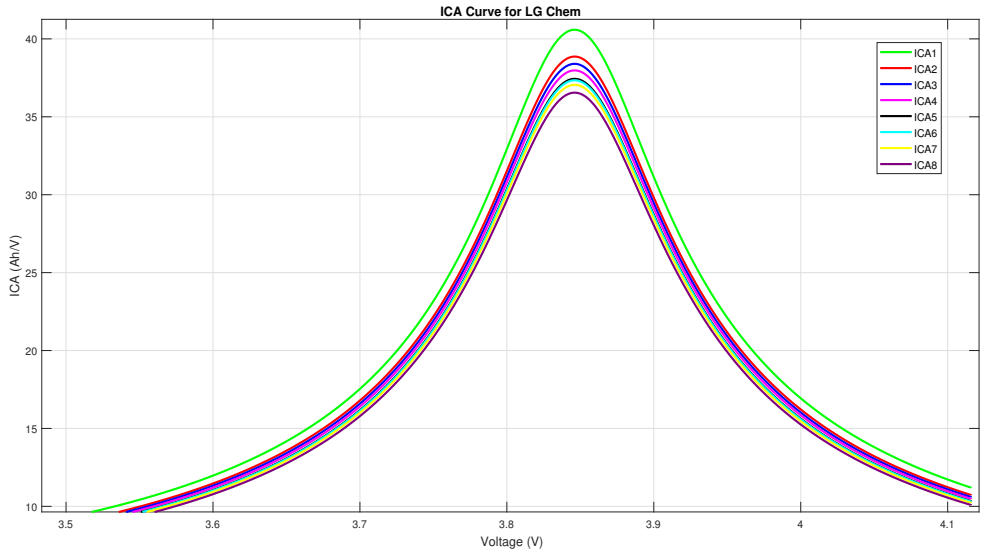

Figure 4.5: ICA curve for Model 2

The OCV curve and ICA plot for Model 3 are shown in Figure 4.6 and 4.7, respectively. ICA peaks for the polynomial models accurately display capacity loss for each test. The peaks do not show any shift due to lack of enough information gathered by the OCV models.

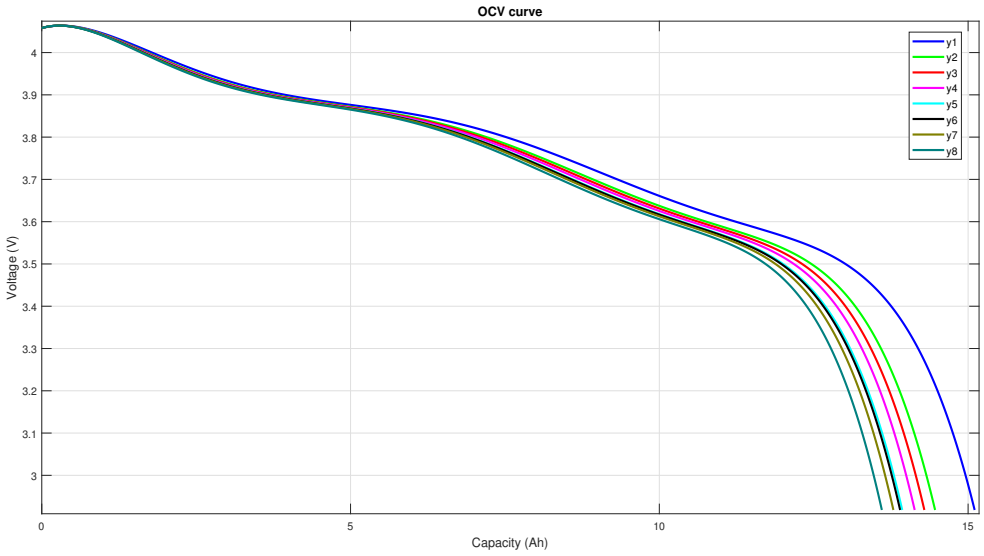

Figure 4.6: OCV curve for Model 3

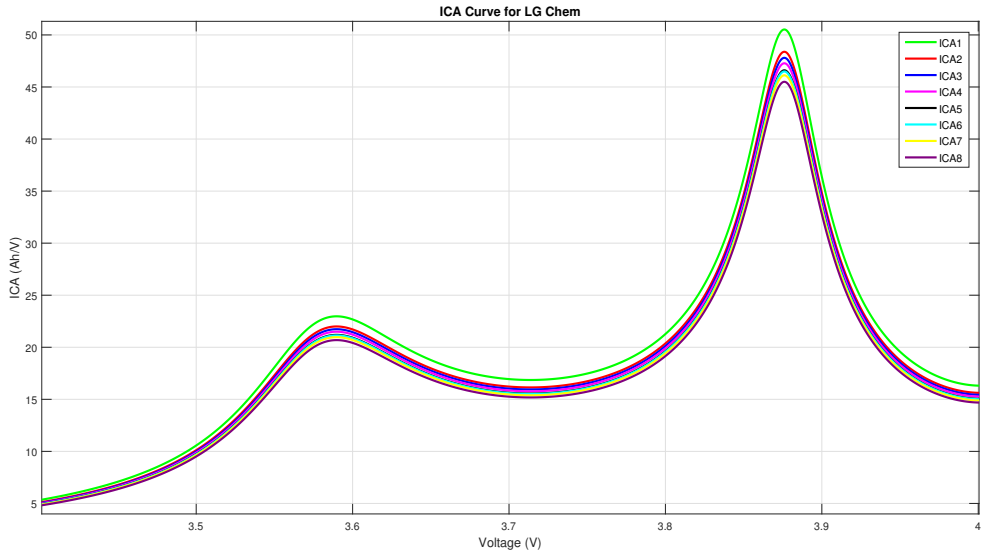

Figure 4.7: ICA curve for Model 3

Table 4.1: Calculation for capacity test data

(a) **Capacity Estimation for Model 1**

Test	Measured Capacity (Ah)	Estimated Capacity (Ah)	Error(%)
test 1	15.1064	16.3271	8.081
test 2	14.466	15.587	7.749
test 3	14.2922	15.3867	7.658
test 4	14.1356	15.2064	7.575
test 5	13.9339	14.9755	7.475
test 6	13.8997	14.9381	7.471
test 7	13.7907	14.8115	7.402
test 8	13.6039	14.5991	7.316

(b) **Capacity Estimation for Model 2**

Test	Measured Capacity (Ah)	Estimated Capacity (Ah)	Error(%)
test 1	15.1064	15.1064	0.0655
test 2	14.466	14.466	0.0691
test 3	14.2922	14.2822	0.07
test 4	14.1356	14.1256	0.0707
test 5	13.9339	13.9238	0.0725
test 6	13.8997	13.8897	0.0719
test 7	13.7907	13.7806	0.0732
test 8	13.6039	13.5938	0.0742

(c) **Capacity Estimation for Model 3**

Test	Measured Capacity (Ah)	Estimated Capacity (Ah)	Error(%)
test 1	15.1064	15.1064	0.0001
test 2	14.466	14.4663	0.0021
test 3	14.2922	14.2925	0.0021
test 4	14.1356	14.1285	0.0503
test 5	13.9339	13.9377	0.0273
test 6	13.8997	13.9001	0.0029
test 7	13.7907	13.7899	0.0058
test 8	13.6039	13.6085	0.0338

Table 4.1 displays the calculation of estimated capacity for each OCV model. The inaccurate OCV-SOC curve produced from Model 1 equation translates into ICA peaks that are ended abruptly. This inaccuracy is seen in the calculation of estimated capacity. The estimated error is higher as a result. On the other hand, polynomial models performed remarkably. The estimated error computed for the models is <0.1% while it is much less for Model 3. The estimated OCV-SOC curve using Model 3 shown in Figure 4.6 depicts smooth transitions corresponding to the li-ion intercalation\de-intercalation process. Accuracy of the polynomial model for capacity fade estimation can be attributed to the higher quality test data obtained from the cycler.

4.5 Reduced Data: Implementation of ICA

The characterization test for LG Chem cell consists of a capacity test and an HPPC test. The HPPC test, as mentioned earlier, is a pulse test that discharges the battery in decrements of 10% SOC. The test is performed at 2C rate i.e., 30A discharge current. Each pulse discharge is followed by rest period that raises the voltage to its OCV value. The HPPC test is performed for the entire voltage range. To investigate performance with less data, the HPPC test data is considered only for SOC up to 50%. Therefore, this mimics the analysis done in Chapter 3 using the mRPT, where in this case we think of the reduced HPPC data as "mRPT". Since we did not have control over how the test data was taken, this is as close as we could achieve the "mRPT" reduced test data.

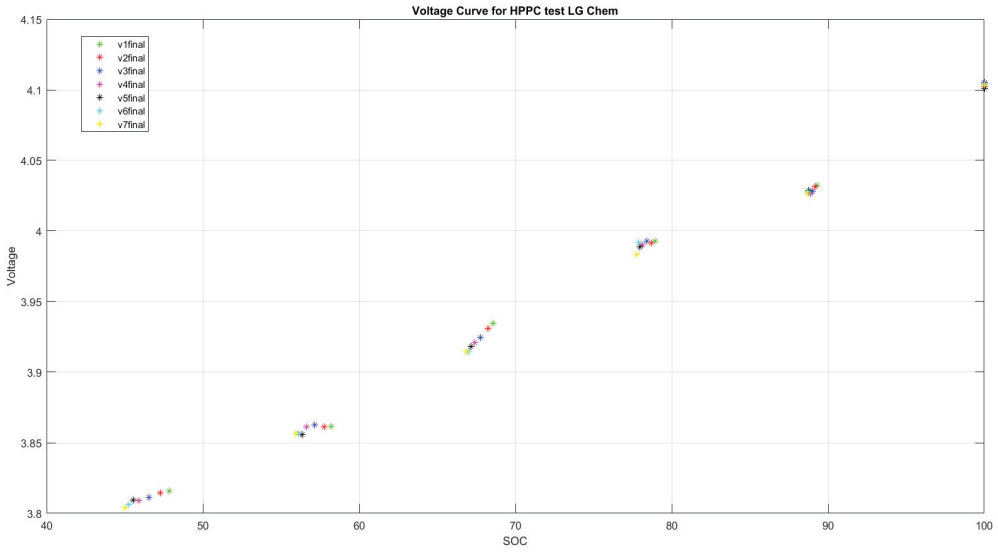

Figure 4.8: OCV data points from rHPPC test

The test data henceforth labeled as rHPPC, to denote reduced data, used for the estimation is reduced to 5 pulses that drops the SOC from 100% to 50%. This data set is then processed for the estimation of capacity using the IC analysis method. The OCV data points for each pulse are extracted from the voltage data set. The OCV value at the end of the rest

period is taken to be the actual OCV value corresponding to the SOC values. Similarly, all the OCV points are extracted from the pulse and their corresponding SOC values are noted. As the capacity degrades in the cell the SOC value tends to shift to a lower value due to the decrease in the total charge accumulated over the pulse. Figure 4.8 shows the shift in the data points as the cell is cycled before each characterization test is performed. The OCV value drops lower for each SOC value which indicates capacity loss.

In addition to this, the OCV voltage obtained for IC analysis is the sum of the OCV values extracted from the test data after each rest period and the drop in voltage due to the internal resistance of the cell. Therefore,

$$V_{oc} = V_T - iR_o \tag{4.1}$$

where V_{oc} is the final OCV value, V_T is the OCV value extracted from the test data, R_o is internal resistance calculated to fit the Randalls model. The OCV-SOC data points are used for OCV curve estimation using an OCV model that is nonlinear in the parameters. The OCV model used for LG Chem cell data is the same as the model used for mRPT data in the last chapter. The parameters are estimated through nonlinear least squares. Following this, OCV data points are generated from SOC values calculated using a coulomb counting method for discharge current data. Similarly, capacity data points are created from charge accumulation at each time period. A ratio of the increments of voltage and capacity produces ICA values. The ICA curve is analyzed for capacity estimation.

4.6 Capacity estimation for rHPPC test

IC analysis of the ICA curve for the rHPPC data is shown in Figure 4.10. The ICA curve for the rHPPC test is similar to the curve obtained from Model 2 equation for the capacity test data. The curve shows the desired drop in the magnitude of each ICA peak, corresponding to the capacity loss after each set of aging cycles. Following this, the ICA curve is evaluated

for estimation in the capacity as the cell degrades. The estimated capacity is calculated and the estimation error for the model is calculated to check for accuracy. Figure 4.9 shows the OCV curve estimated from the non-linear model.

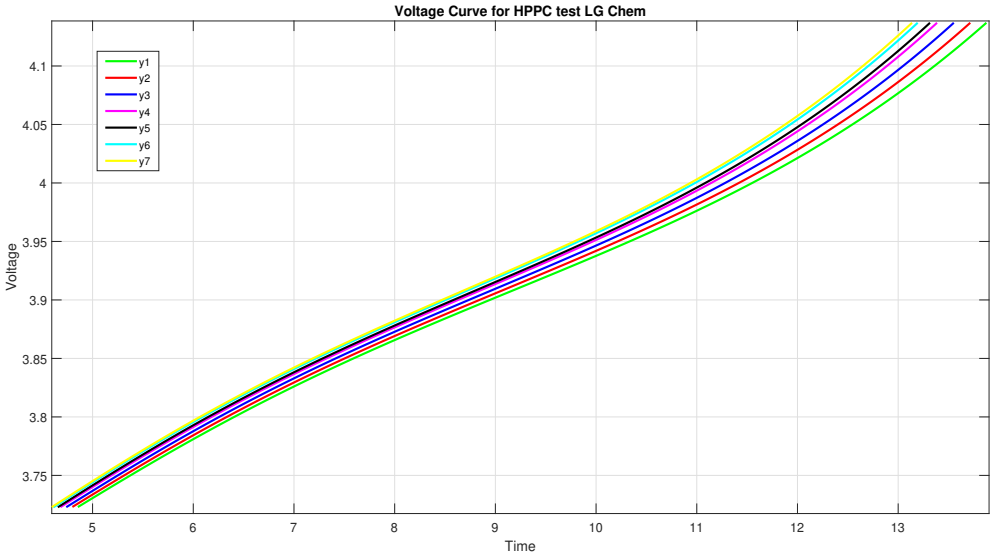

Figure 4.9: OCV curve from rHPPC test

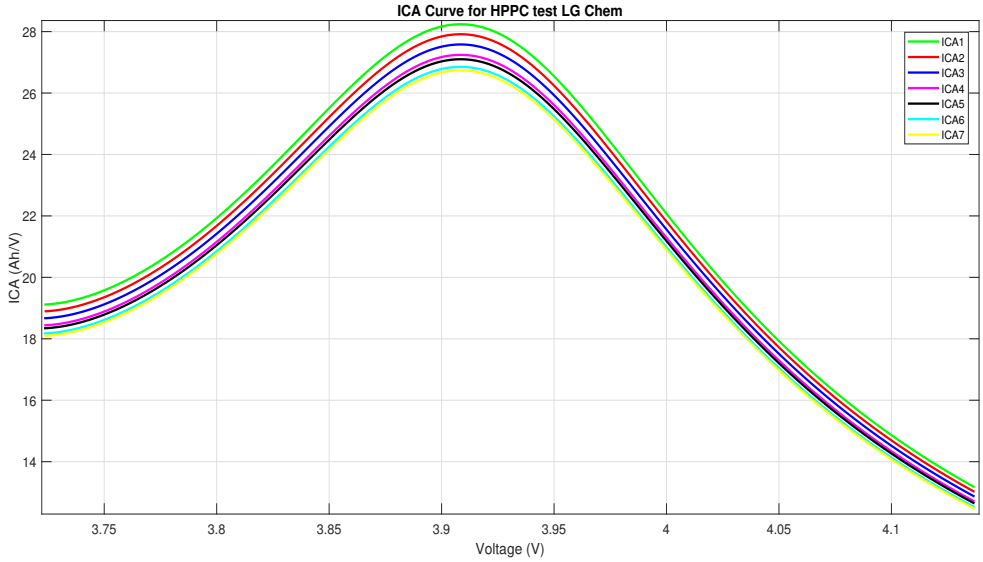

Figure 4.10: ICA curve from rHPPC test

Table 4.2: ICA calculation for rHPPC test data

Test	Measured Capacity (Ah)	Estimated Capacity (Ah)	Error(%)
test 1	14.466	14.4661	0.0001
test 2	14.2922	14.2986	0.0447
test 3	14.1356	14.1076	0.1979
test 4	13.9339	13.9333	0.0041
test 5	13.8997	13.8635	0.2606
test 6	13.7907	13.7392	0.3737
test 7	13.6039	13.6740	0.5150

Table 4.2 displays the calculation of estimated capacity for each OCV model. The measured capacity is the true capcaity of the battery. The capacity estimation for the LG Chem cell using the rHPPC test is challenging since the estimation is performed using just 6 data points. The OCV model used for the estimation of capacity in the thesis performed well due to the nonlinear parametric term present in the Equation 3.2. The exponential term used in OCV model is able to derive crucial information on nonlinear characteristics of the OCV curve from the data points and then translate the information into corresponding ICA peaks. The estimated value is accurate with estimation error of $<1\%$.

4.7 Summary

The estimation of capacity fade in a higher grade LG Chem cell was computed. OCV-SOC curves and the ICA curves were accurately estimated from each OCV model. The cell tests provided better quality of test data compared to the Turnigy battery pack, that resulted in better accuracy in capacity estimation. The ICA calculation for the rHPPC test was able to successfully estimate the capacity fade in the cell from fewer data points which is the main objective of the thesis. Moreover, the capacity estimated for the rHPPC test compared well with the capacity estimated for capacity test and the measured capacity, given the vast difference in the test data size.

CHAPTER 5

CONCLUSION AND FUTURE WORK

5.1 Conclusion

Li-ion batteries have proven to be the leading source of energy for powering EVs. It is crucial to monitor the efficiency of the batteries in order to derive maximum performance. The efficiency of these li-ion batteries correspond to their aging life and capacity. Therefore a battery management system is required to accurately estimate the capacity and aging of the battery and to ascertain longer life. This thesis examines a capacity estimation method using ICA with different OCV models for a lower grade Turnigy battery pack and a high grade single LG Chem cell for set of data obtained from capacity tests, mRPTs and rHPPC tests.

Factors affecting capacity and aging in the battery are discussed in Chapter 1. The process of capacity loss caused by aging cycles and their corresponding effects that result in loss of lithium ion in a battery pack is described. Chapter 1 also discussed the battery pack manufactured by Turnigy and its specifications. Testing equipment such as cycling station, temperature chamber and the software used for the experiments is briefly discussed. A series of testing profiles used for cycling the Turnigy battery pack is explained in detail.

Chapter 2 introduced the technique of incremental capacity analysis for capacity fade estimation. The sequence of lithium ion accumulation at different stages during a charge/discharge for different SOCs is explained in this chapter. The derivative nature of ICA presented a relation between the ICA peak and the plateau region in the OCV curve. Variation in peak height corresponding to capacity loss is observed. A review of ICA and OCV-SOC curves for different batteries like LNMCO, $LiMn_2O_4$, $LiFePO_4$ and LTO described particular characteristics of the battery with different cell chemistry thereby presenting an interesting analysis of battery behavior for different cell chemistry at different stages. The OCV models used in

this thesis expressed the need for smooth data in capacity estimation. Three OCV models are studied and compared for estimation of OCV-SOC curve.

In Chapter 3, results of capacity estimation for the Turnigy battery pack are presented. OCV-SOC curves estimated from the $Q_i$test for each OCV model are compared. The ICA curves obtained from the three OCV models are presented. Results for the capacity estimation at four different temperatures 0°C, 10°C, 25°C and 50°C are discussed. A comparison of estimated capacity and estimation error calculated for each model at different temperatures is presented, and performance analysis of the battery for different models is discussed in detail. The analysis is performed for different temperatures and their effect on capacity is examined. An approach for capacity estimation using less data from the mRPT is proposed. A nonlinear parametric model equation for estimating OCV-SOC curve from mRPT data is presented, and the OCV-SOC curve and ICA curve for the battery are discussed. ICA curves for each test showed no change in the peak height corresponding to the fade in capacity. Result for capacity estimation from the model is discussed and summarised.

Chapter 4 introduced LG Chem battery test data used for this thesis. Various testing profiles executed for the aging process in LG Chem are discussed. Aging cycle described the characteristic charge depleting and charge sustaining sub-cycles run on the battery. Comparison of capacity estimation for three OCV models using capacity test data is discussed. ICA and OCV-SOC curves for each model are illustrated and compared. Capacity estimation and the estimation error for each model is shown in the table and a summary on accuracy of different models is presented. The first half of the HPPC test termed as "reduced-hppc or rhppc" mimicking a mRPT is evaluated for capacity estimation. A nonlinear parametric OCV model from mRPT is used for the estimation, and the OCV-SOC curve estimated using less data points and the ICA curve corresponding to the OCV-SOC curve are illustrated. The IC analysis for capacity fade is performed. Calculation for capacity estimation shown in the table is discussed and the accuracy of the estimation is evaluated.

5.2 Contributions

The ICA analysis for capacity fade estimation using $Q_i$test achieved in this thesis has been seen in the literature. However, the amount of data from the $Q_i$test is vast and requires years of testing to obtain such data. Furthermore, Q_i tests run at lower C rates and take much longer to execute and consist of a huge amount of data points. In practice, estimation of capacity using such data is impractical. The main contribution of the thesis is to estimate capacity fade in a battery using much less data from the mRPT. The mRPT is executed at higher C rates therefore discharges the battery faster and the amount of data obtained from the test is much less compared to the $Q_i$tests. The OCV-SOC curve is modeled using only six data points for SOC ranging from 100% to 50%. On comparing with the $Q_i$test that uses around 3000 data points for SOC ranging from 100% to 0%, mRPT generates only 180 data points during the discharge cycle for SOC 100% to 50%, which is significantly less. Furthermore, modeling a non-linear parametric OCV model using 6 data points for an accurate OCV-SOC curve is a challenge. In this thesis, capacity estimation of error less than 1% for LG Chem cell from less data points was achieved using a OCV model equation with nonlinear parameter.

5.3 Future Work

This thesis discussed incremental capacity analysis, which was shown to accurately estimate capacity fade. However, charge accumulation for generating capacity points is based on a coulomb counting method which is prone to current measurement error. Therefore a more robust method for calculating charge accumulation is required for improving the ICA curve required for IC analysis.

Significant improvement can be made in OCV models. Accurate estimation of OCV curve is required to extract crucial information on the characteristics of the OCV-SOC curve. A

non-linear parametric equation that closely estimates the non-linear characteristics of the OCV-SOC curve can be developed in order to improve the estimation accuracy. Additionally, synthetic data can be generated between the OCV points extracted from the test data by implementing unsupervised learning algorithm that is trained on the OCV data obtained from Q_0test. These additional data points generated can be used to improve the estimation accuracy of OCV model. Furthermore, temperature and internal resistance could be incorporated as an input to the OCV model in order to model the effect of temperature variation and change in internal resistance in the battery.

REFERENCES

BatteryUniveristy (2017). Bu-410: Charging at high and low temperatures. Available at `http://batteryuniversity.com/learn/article/charging_at_high_and_low_temperatures`.

Carnovale, A. (2017). Investigation into the effect of thermal management on the capacity fade of lithium-ion batteries. Master's thesis, University of Waterloo.

Cordoba-Arenas, A., S. Onori, Y. Guezennec, and G. Rizzoni (2015). Capacity and power fade cycle-life model for plug-in hybrid electric vehicle lithium-ion battery cells containing blended spinel and layered-oxide positive electrodes. *Journal of Power Sources 278*, 473–483. "Reprinted from Journal of Power Sources, 278, Andrea Cordoba-Arenas, Simona Onori, Yann Guezen-nec, Giorgio Rizzoni, Capacity and power fade cycle-life model for plug-in hybrid electric vehicle lithium-ion battery cells containing blended spinel and layered-oxide positive electrodes, 473-483, Copyright (2017), with permission from Elsevier".

Dubarry, M. and B. Y. Liaw (2009). Identify capacity fading mechanism in a commercial lifepo 4 cell. *Journal of Power Sources 194*(1), 541–549.

Dubarry, M., V. Svoboda, R. Hwu, and B. Y. Liaw (2006). Incremental capacity analysis and close-to-equilibrium ocv measurements to quantify capacity fade in commercial rechargeable lithium batteries. *Electrochemical and solid-state letters 9*(10), A454–A457.

Dubarry, M., V. Svoboda, R. Hwu, and B. Y. Liaw (2007). Capacity loss in rechargeable lithium cells during cycle life testing: The importance of determining state-of-charge. *Journal of Power Sources 174*(2), 1121–1125.

Groot, J. (2012). State-of-health estimation of li-ion batteries: Cycle life test methods. Master's thesis, Chalmers University of Technology.

Groot, J. (2014). *State-of-health estimation of Li-ion batteries: Ageing models*. Ph. D. thesis, Chalmers University of Technology.

Guo, L. (2015). *Modeling and verification of a lithium iron phosphate battery pack system for automotive applications*. The University of Texas at Dallas.

Lu, L., X. Han, J. Li, J. Hua, and M. Ouyang (2013). A review on the key issues for lithium-ion battery management in electric vehicles. *Journal of power sources 226*, 272–288.

Plett, G. L. (2004). Extended kalman filtering for battery management systems of lipb-based hev battery packs: Part 3. state and parameter estimation. *Journal of Power sources 134*(2), 277–292.

Pyne, M., B. J. Yurkovich, and S. Yurkovich (2017). Capacity fade estimation using supervised learning. In *Control Technology and Applications (CCTA), 2017 IEEE Conference on*, pp. 872–878. IEEE.

Ramadass, P., B. Haran, R. White, and B. N. Popov (2003). Mathematical modeling of the capacity fade of li-ion cells. *Journal of Power Sources 123*(2), 230–240.

Roscher, M. A., J. Assfalg, and O. S. Bohlen (2011). Detection of utilizable capacity deterioration in battery systems. *IEEE Transactions on vehicular technology 60*(1), 98–103.

Scrosati, B. and J. Garche (2010). Lithium batteries: Status, prospects and future. *Journal of Power Sources 195*(9), 2419–2430.

Vetter, J., P. Novk, M. Wagner, C. Veit, K.-C. Mller, J. Besenhard, M. Winter, M. Wohlfahrt-Mehrens, C. Vogler, and A. Hammouche (2005). Ageing mechanisms in lithium-ion batteries. *Journal of Power Sources 147*(1), 269 – 281. "Reprinted from Journal of Power Sources, 147, J. Vetter, P. Novk, M.R. Wagner, C. Veit, K.-C. Mller, J.O.Besenhard, M. Winter, M. Wohlfahrt-Mehrens, C. Vogler, A. Hammouche, Ageing mechanisms in lithium-ionbatteries, 269-281, Copyright (2017), with permission from Elsevier".

Wang, Q., P. Ping, X. Zhao, G. Chu, J. Sun, and C. Chen (2012). Thermal runaway caused fire and explosion of lithium ion battery. *Journal of power sources 208*, 210–224.

Weng, C., X. Feng, J. Sun, and H. Peng (2016). State-of-health monitoring of lithium-ion battery modules and packs via incremental capacity peak tracking. *Applied Energy 180*, 360–368.

Weng, C., J. Sun, and H. Peng (2013). An open-circuit-voltage model of lithium-ion batteries for effective incremental capacity analysis. In *ASME 2013 Dynamic Systems and Control Conference*, pp. V001T05A002–V001T05A002.

Weng, C., J. Sun, and H. Peng (2014). A unified open-circuit-voltage model of lithium-ion batteries for state-of-charge estimation and state-of-health monitoring. *Journal of power Sources 258*, 228–237.

Zhang, C., J. Jiang, L. Zhang, S. Liu, L. Wang, and P. C. Loh (2016). A generalized soc-ocv model for lithium-ion batteries and the soc estimation for lnmco battery. *Energies 9*(11), 900.

BIOGRAPHICAL SKETCH

Suvrat Ramasubramanian received his Bachelor of Technology (B.Tech.) degree in electronics engineering from NMIMS University, Mumbai, India, in June 2014. Later he began his graduate school at University of Texas at Dallas, Richardson, Dallas, Texas, USA in Spring 2016 for Masters of Science in electrical engineering. Prior to joining graduate school, he interned at Indian Institute of Technology, Madras, India, on projects for designing a smartphone based microscope and designing current sensors circuit for rapid chloride precipitation test used in civil engineering.

CURRICULUM VITAE

Suvrat Ramasubramanian

November 10, 2017

Contact Information:

Department of Systems Engineering
The University of Texas at Dallas
800 W. Campbell Rd.
Richardson, TX 75080-3021, U.S.A.

Email: sxr154231@utdallas.edu

Educational History:

B.Tech., Electronics Engineering, NMIMS University, 2014
M.S., Electrical Engineering, The University of Texas at Dallas, 2017

Employment History:

Teaching Assistant - Linear systems, The University of Texas at Dallas, September 2016 – December 2016